



## Spinel ferrites gas sensors: a review of sensing parameters, mechanism and the effects of ion substitution

Muasya Alex Njoroge, Nixon Mutwiri Kirimi & Kamweru Paul Kuria

To cite this article: Muasya Alex Njoroge, Nixon Mutwiri Kirimi & Kamweru Paul Kuria (2021): Spinel ferrites gas sensors: a review of sensing parameters, mechanism and the effects of ion substitution, *Critical Reviews in Solid State and Materials Sciences*, DOI: [10.1080/10408436.2021.1935213](https://doi.org/10.1080/10408436.2021.1935213)

To link to this article: <https://doi.org/10.1080/10408436.2021.1935213>



Published online: 03 Sep 2021.



Submit your article to this journal [↗](#)



Article views: 554



View related articles [↗](#)



View Crossmark data [↗](#)

# Spinel ferrites gas sensors: a review of sensing parameters, mechanism and the effects of ion substitution

Muasya Alex Njoroge, Nixon Mutwiri Kirimi, and Kamweru Paul Kuria

Department of Physical Sciences, Chuka University, Chuka, Kenya

## ABSTRACT

There is an increasing demand of highly sensitive, stable and highly selective gas sensors to detect toxic gases. This is inspired by the need to monitor the concentration of these gases in order to guarantee humans, animals and environmental safety. Metal ferrites ( $AFe_2O_3$ , where A is a metal) based sensors are paramount in this field of sensing. Among the gases detectable using metal ferrites includes carbon monoxide (CO), liquefied petroleum gas (LPG), hydrogen sulfide ( $H_2S$ ), petrol and methane ( $CH_4$ ). This reviews presents various parameters which plays key role in the design of ferrite gas sensors. They include; operating temperatures, dopants, grain size, particle size, selectivity, surface area, concentration of the gas, sensitivity as well as recovery time. In addition, the various methods which are used to synthesize ferrite gas sensors are briefly explained. Key considerations in the designing of excellent ferrite gas sensors such as calcination temperature, working temperature, dopants, and concentration as well as optimization condition among others are outlined. In addition this paper reviews the various metal ferrites such as nickel ferrites and nickel doped ferrites, cobalt and cobalt doped ferrites, zinc and zinc doped ferrites, magnesium and magnesium doped ferrites among others that have been researched as gas sensors.

## KEYWORDS

Ferrites; gas sensors; selectivity; surface area; sensing parameters; sensing mechanism; adsorption

## Table of contents

1. Introduction	2
2. Parameters of gas sensing	4
2.1. Pore structure	4
2.2. Surface area	4
2.3. Crystallite size, grain size and particle size	4
2.4. Operating temperature	6
2.5. Sensitivity	7
2.6. Selectivity	7
2.7. Dopants (influence to sensitivity, selectivity and operational temperature)	7
2.8. Response characteristics	7
2.9. Sensor resistance to gas concentration	8
2.10. Fabrication and morphology of gas sensor	8
2.11. Phase formation	8
2.12. Surface phenomena and gas sensing mechanism	8
2.12.1. Adsorption	8
2.12.2. Surface state	9
2.12.3. Mechanism of gas sensing	9
3. Gas sensing mechanism in ferrites	9
3.1. P-type spinel ferrite gas sensors	10
3.2. N-type spinel ferrite gas sensors	10
3.3. Substituted and mixed ferrites sensors	11
3.4. Spinel ferrite humidity sensor	11

<b>4. Ferrite gas sensors</b> .....	11
4.1. Nickel ferrite and nickel doped ferrite .....	12
4.1.1. Nickel ferrites .....	12
4.1.2. Nickel doped ferrites .....	12
4.2. Cobalt ferrite and cobalt doped ferrites .....	13
4.2.1. Cobalt ferrites .....	13
4.2.2. Cobalt doped ferrites .....	13
4.3. Zinc ferrites and zinc doped ferrites .....	14
4.3.1. Zinc ferrites .....	14
4.3.2. Zinc doped ferrites .....	15
4.4. Copper ferrites and copper doped ferrites .....	15
4.4.1. Copper ferrites .....	15
4.4.2. Copper doped ferrites .....	15
4.5. Cadmium ferrites and cadmium doped ferrites .....	16
4.5.1. Cadmium ferrites .....	16
4.5.2. Cadmium doped ferrites .....	16
4.6. Magnesium ferrites and magnesium doped ferrites .....	16
4.6.1. Magnesium ferrites .....	16
4.6.2. Magnesium doped ferrites .....	17
4.7. Manganese ferrites and manganese doped ferrites .....	17
4.7.1. Manganese ferrites .....	17
4.7.2. Manganese doped ferrites .....	17
4.8. Lithium and lithium doped ferrites .....	18
<b>5. Methods of synthesis of gas sensing spinel ferrites</b> .....	18
5.1. Sol-gel auto-combustion method .....	18
5.1.1. Reductant to metal salt ratio .....	19
5.1.2. Combustion process chemical additives (CPCA) .....	20
5.2. Co-precipitation method .....	20
5.3. Solid-state reaction method .....	21
5.4. Wet chemical method .....	21
5.5. Molten-salt method .....	21
<b>6. Conclusion</b> .....	21
<b>References</b> .....	22

## 1. Introduction

The air that we breathe comprises of different chemical species, some of them being useful while others being dangerous. In recent years, presence of toxic and harmful gas pollutants have become an issue of concern.<sup>1</sup> This has created demand for the detection and monitoring of these gases. By design, a gas sensor should perform two crucial functions i.e. the receptor and transducer functions. The former function is the ability to recognize (by interactions such as adsorption, chemical or electrochemical reaction) particular gas species while the latter is that ability to transduce the gas recognition into a sensing signal (e.g. electrical resistance change, capacitance, electromotive force, resonant frequency, optical absorption or emission, work function, mass, optical characteristics, reaction energy released by the gas/solid interaction, magnetic (magneto-optical Kerr effect) among others.

Research in gas sensors is geared to enhance the two functions,<sup>2</sup> i.e. improvement of the receptor function usually related to selectivity and enhancement of transducer function which is directly related to the sensitivity of a gas sensors.<sup>3</sup> There are different sensing techniques used to achieve the two functions, consequently giving rise to different sensor techniques that includes catalytic gas sensors,<sup>4</sup> electrochemical gas sensors,<sup>5</sup> optical gas sensors,<sup>6</sup> thermal conductivity gas sensors<sup>7</sup> and acoustic gas sensors.<sup>8,9</sup>

Basically almost any metal oxide could be a basis for solid-state gas sensor, if it is prepared as a sufficiently fine dispersed porous substance with properties controlled by surface states. However, for implementation of all sensing requirements, a material for solid-state gas sensors has to exhibit a specific combination of physical-chemical properties. Therefore not every metal oxide can be corresponded these requirements. Among the earliest experimented metal oxides as gas

sensors were ZnO powders, TiO<sub>2</sub> and SnO<sub>2</sub> after realization that their electrical conductivity changed with the composition of the gas atmosphere.<sup>10</sup> In the recent past, the semiconducting metal oxide sensors (MOS) are one of the studied group in the field of gas sensing.<sup>11–14</sup> They attract much interest in gas sensing under atmospheric condition as a result of their flexibility in production, large number of detectable gases, low cost as well as simplicity of their use. These materials are able to use either physical or chemical effect to convert any component or concentration of a gas into detectable electric signal. These metal oxide shown to be sensitive toward certain gas species, for example, SnO<sub>2</sub> as H<sub>2</sub>, H<sub>2</sub>S, NH<sub>3</sub>, C<sub>2</sub>H<sub>5</sub>OH, CO and SO<sub>2</sub> sensor<sup>15–17</sup>; ZnO as C<sub>2</sub>H<sub>5</sub>OH, CO, H<sub>2</sub> and NO<sub>3</sub> sensor<sup>18–20</sup>; WO<sub>3</sub> toward N<sub>2</sub> and NH<sub>3</sub> sensing<sup>21–23</sup>; TiO<sub>2</sub>.<sup>24</sup> The fabrication of these sensors mainly uses thick films, pellets as well as thin film technology.<sup>25,26</sup> The fabrication seeks to achieve the aforementioned two main gas sensors functions, as well as their durability.

Composite metal oxides usually show better gas response than the single component if the catalytic actions of the components complement each other<sup>27</sup> e.g. binary oxide<sup>28,29</sup> and ternary oxide.<sup>30</sup> Noble metal additives with high-effective oxidation catalytic activity can be used to enhance the sensitivity of pure metal oxides due to the “spillover effect,”<sup>27,31</sup> e.g. addition of silver,<sup>32</sup> Lead, Platinum and Gold,<sup>33</sup> silver, Gold, Platinum and Lead.<sup>34</sup> Generally the structure of the metal oxide is very important in achieving selectivity and sensitivity functions; high surface areas are necessary to obtain highly-dispersed catalyst particles and provide large reaction contact area between gas sensing materials and target gases<sup>35,36</sup>; Porous structure increases surface area,<sup>37,38</sup> small grain size is useful to enhance the sensitivity<sup>39</sup>; surface engineering to achieve right crystallographic facets improves recovery speed.<sup>4,41</sup>

There exist some drawbacks for some metal oxide gas sensors which include; poor long-term stability which can be reduced further when working under critical condition thereby limiting them for practical application<sup>42,43</sup>; poor selectivity<sup>44</sup> for example SnO<sub>2</sub><sup>16</sup>; high working temperature for example ZnO working at 400–500 °C.<sup>45</sup> Among all the metal oxide sensors, spinel type oxides with the formula AB<sub>2</sub>O<sub>4</sub> (where A is a divalent metal and B a trivalent one, and located as shown in Figure 1) play an important role in gas sensing. They have been studied widely for the detection of oxidizing as well as reducing gases depending upon the type of conductivity possessed by the

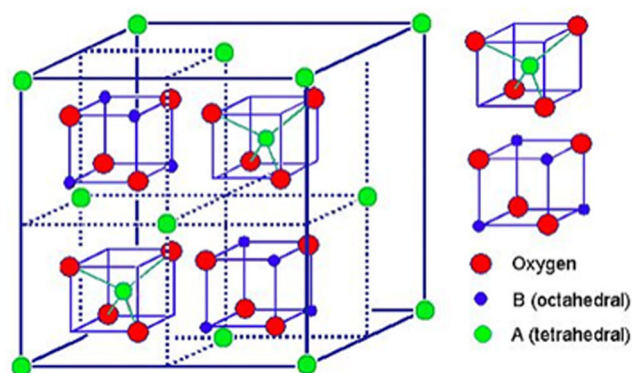


**Figure 1.** The spinel structure of ferrites indicating the tetrahedral and octahedral sites. Figure obtained from Issa et al.<sup>46</sup> The divalent All cations occupy 1/8th of the tetrahedral voids, whereas the trivalent BIII cations occupy one half (1/2) of octahedral voids.

material.<sup>11,47</sup> Spinel ferrites have been widely studied for the sensing of both reducing gases and oxidizing gases. The suitability of ferrite as gas sensors is their capability of fine tuning of electrical properties.<sup>11</sup> In addition, ferrites also have oxygen vacancies which modify the conduction properties and hence the electrical response of the sensor.<sup>12</sup> The major advantage of spinel ferrite in comparison with other sensor material involving single metal oxide semiconductor is their capability of adjusting the type of conductivity and resistance value by changing the positive ions position and calcination condition.<sup>47</sup>

The importance of spinel ferrites in sensing field is that a variety of transition metal cations can be incorporated in the lattice of the parent magnetite structure.<sup>45</sup> In the structure they contain 8 tetrahedral coordinated (A) sites and 16 octahedral coordinated (B) sites. The conduction of these sensors occurs via the transfer of electrons or holes between equal cations located in octahedral sites.<sup>48</sup> Compared to other traditional metal oxide semiconductor spinel type ferrite have lots of advantages which include; capability of fine tuning of electrical properties due to oxygen vacancies which modify the conduction properties and hence the electrical response of the sensor.<sup>1,49,50</sup>

Their selectivity for some gases are comparatively better than other semiconducting oxide; they have controllable high thermodynamic stability, high corrosion resistance, low magnetic transition temperature as well as low melting point.<sup>51,52</sup> In addition ferrites are simple to synthesize, have low cost reproducible and as well when compared to other gas sensors have structural and compositional flexibility and hence place them in a better place in the field of gas sensor technology. This review focuses on the Spinel Ferrites

Gas Sensors, their sensing parameters, mechanism and the effects of ion substitution.

## 2. Parameters of gas sensing

The parameters crucial in gas sensing, and especially using ferrites sensors are elaborated in this part. Various metal ferrites used as sensors for various gases and their optimized parameters are summarized in Table 1.

### 2.1. Pore structure

Pores are the void spaces found between the ceramic grains and can be categorized as open passage pores, open dead-end pores and internal or sealed pores.<sup>53</sup> Pores can be rectangular, square, split, cylindrical among others depending on the shapes of cross section. The pore size can be classified as microspores (about 2 nm), mesoporous (between 2–200 nm) and macropores (the average cross section diameter about 200 nm). Porosity is the ratio of total pores per volume.

$$P = \frac{V_p}{V} \quad (1)$$

where  $V_p$  the total is pores volume and  $V$  is the volume of the body.

Porosity influences sensitivity since the adsorption of gas analyte takes place at the porous pores at the surface of the sensor.<sup>54</sup> Ferrite with open pore exhibit improved sensitivity. High porosity of  $\text{CO}_{1-x}\text{Ni}_x\text{Fe}_2\text{O}_4$ <sup>55</sup> sensor influenced its sensitivity toward ethanol and CO. Large number of pore in  $\text{LaFe}_2\text{O}_4$  LPG sensor<sup>56</sup> influences its sensitivity. The open pores allow faster adsorption of test gas analyte and hence faster response. Superior gas sensing properties toward acetone using porous  $\text{CuFe}_2\text{O}_4$  was reported.<sup>57</sup> This was attributed to the porous nanostructure and secondly due to the surface of the  $\text{CuFe}_2\text{O}_4$  nanospheres. More recent studies on ferrites nanoparticles,<sup>58</sup> nanorods<sup>59,60</sup> nanospheres,<sup>61</sup> nanocubes,<sup>59</sup> nanoparticulate thin films<sup>62</sup> and nanoplates<sup>63</sup> are in agreement on the benefit of higher porosity in gas sensing.

### 2.2. Surface area

The surface area plays important role in gas sensing in that porous metal oxides (see Eq. (2)) with large surface area gives high sensitivity within certain limit.<sup>64</sup> Specific surface area,  $A$ , refers to the ratio of total ceramic surface to its mass.

$$A = \frac{S}{m} \quad (2)$$

where  $S = S_n$  (total surface area of ceramic body surface) +  $S_p$  (surface of internal pores).

Nanoparticles with large surface area to volume ratio improves sensitivity of gas as the interaction of the gas analyte and the sample mainly appears on the surface.<sup>53</sup> Rezlescu et al.<sup>65</sup> established specific area of ferrite using Eq. (3).

$$A = \frac{S}{Vd} = \frac{6}{d.D_m} \quad (3)$$

where  $S$  is surface area of the particle,  $V$  is the volume of the particle,  $d$  is the bulk density,  $D_m$  is the average grain size (see § 2.3) and the number 6 is the shape factor. Generally, materials with smaller size of the particle as well as the large specific area enhance gas sensing process. Cao et al.<sup>66</sup> prepared ferrites  $\text{MFe}_2\text{O}_4$  ( $M = \text{Fe}, \text{Co}, \text{Ni}, \text{Mg}, \text{Cd}$  and  $\text{Zn}$ ) materials of different morphologies. They found that  $\text{ZnFe}_2\text{O}_4$  displayed best response which was as a result of its intrinsic semiconductor characteristic as well as its suitable porosity which have large surface specific surface area of  $67.14 \text{ m}^2\text{g}^{-1}$  compared to the lowest of  $10.52 \text{ m}^2\text{g}^{-1}$  for the  $\text{NiFe}_2\text{O}_4$ .

### 2.3. Crystallite size, grain size and particle size

Three terms, crystallite size, grain size and particle sizes do not mean the same thing. Crystallite refers to the size of the one crystal inside the particle or grain, and is determined using the Debye Scherer formula,<sup>67,68</sup> Eq. (4).

$$D_c = \frac{k\lambda}{\beta \cos \theta} \quad (4)$$

where  $D_c$  is crystallite size,  $\beta$  is the full width at half maximum intensity of peak at an angle  $\theta$ ,  $k$  is a constant and  $\lambda$  is the wavelength of the x-ray source. Several crystals make up a grain, sometimes the crystal size may match the grain size, and it established in some studies that more often, the grain size is much larger than crystallite size.<sup>69,70</sup> The term particle size is used when the size of single crystal is of less than about  $10^{-5} \text{ cm}$ , the limit at which the broadening of the X-ray diffraction lines occurs.<sup>71</sup> Generally, ferrites with smaller grain size, smaller crystallite size and open pores exhibit improved sensitivity. Smaller grain results to an increase of the grain boundary surface which in turn result to high resistivity.<sup>65</sup>  $\text{MgFe}_2\text{O}_4$  sensor exhibited the highest response with good selectivity and speedy response-recovery behavior to ethanol which was attributed by its smaller crystallite

Table 1. Parameters in gas sensing using ferrites.

Ferrites	Synthesized methods	Temperature		Operating	Sensitivity	Selectivity	Concentration (ppm)	Crystallite size (nm)	Particle size (nm)	Response time	Recovery time	References
		Calcination	Calcination									
Ag-NiFe <sub>2</sub> O <sub>4</sub>	Solid state	800 °C	800 °C	–	43	Acetone	–	–	–	1 s	≈10 s	164
CdFe <sub>2</sub> O <sub>4</sub>	Sol-gel self-auto-combustion	1000 °C	1000 °C	350 °C	–	LPG, C <sub>2</sub> H <sub>5</sub> OH and acetone	150	300	–	–	–	73
CdFe <sub>2</sub> O <sub>4</sub>	Oxallate Co-precipitate	–	–	350 °C	85% 35% 30%	C <sub>2</sub> H <sub>5</sub> OH LPG C <sub>2</sub> H <sub>5</sub> OH	–	30	–	200–250 s	250–300 s	207
CdFe <sub>2</sub> O <sub>4</sub>	Chemical co-precipitate	600 °C and 800 °C	600 °C and 800 °C	380 °C	90%	C <sub>2</sub> H <sub>5</sub> OH	200	15	–	15 s	35 s	206
Co <sub>0.01</sub> Mn <sub>0.02</sub> Fe <sub>1.98</sub> O <sub>4</sub>	Self-combustion	1000 °C	1000 °C	230 °C	–	C <sub>2</sub> H <sub>5</sub> OH, CH <sub>4</sub> , LPG	–	100–500	0.1 μm	–	–	145
Co <sub>0.8</sub> Ni <sub>0.2</sub> Fe <sub>2</sub> O <sub>4</sub>	Sol gel citrate	600 °C	600 °C	210 °C	–	NH <sub>3</sub>	200	30	25–35	50 s	–	175
Co <sub>1-x</sub> Mn <sub>x</sub> Fe <sub>2</sub> O <sub>4</sub>	Chemical spray pyrolysis	900 °C	900 °C	150 °C	90%	NO <sub>2</sub>	100	45–65	–	1.62	–	176
Co <sub>1-x</sub> Ni <sub>x</sub> Fe <sub>2</sub> O <sub>4</sub>	Co-precipitate	550 °C	550 °C	325 °C	–	CO and C <sub>2</sub> H <sub>5</sub> OH	10–1000	10–20	–	–	–	55
CoFe <sub>2</sub> O <sub>4</sub>	hydrothermal	75 °C	75 °C	150 °C	71.9	C <sub>2</sub> H <sub>5</sub> OH	10	–	15–20	–	–	154
CoFe <sub>2</sub> O <sub>4</sub>	chemical spray pyrolysis	900 °C	900 °C	150 °C	90%	NO <sub>2</sub>	80	200–400	–	5 s	117 s	172
CoFe <sub>2</sub> O <sub>4</sub>	wet chemical	175 °C	175 °C	227 °C	–	NH <sub>3</sub>	25	40	–	–	–	173
CoFe <sub>2</sub> O <sub>4</sub>	Spray pyrolysis	900 °C	900 °C	150 °C	–	NO <sub>2</sub>	5–8	100–200	–	5–9s	130–160s	169
CuFe <sub>2</sub> O <sub>4</sub>	Sol-gel auto-combustion	700 °C	700 °C	80 °C	–	H <sub>2</sub> S	25	32	35.8 ± 5.3 s	51.5 ± 3.4 s	–	200
CuFe <sub>2</sub> O <sub>4</sub>	Sol-gel spin coating	500 °C	500 °C	25 °C	1.96	LPG	500	13	12	60 s	400 s	201
CuFe <sub>2</sub> O <sub>4</sub>	Sol-gel self-autocombustion	1000 °C	1000 °C	350 °C	90%	C <sub>2</sub> H <sub>5</sub> OH, acetone and LPG	150	700	–	3 min	4 min	65
CuFe <sub>2</sub> O <sub>4</sub>	Auto-combustion	600 °C and 900 °C	600 °C and 900 °C	300 °C	–	LPG	1000	≈9–45	40–60	–	–	203
Li <sub>0.5</sub> Sm <sub>x</sub> Fe <sub>2.5-x</sub> O <sub>4</sub>	Sol-gel self-auto-combustion	850 °C	850 °C	60 °C	80–87%	Methanol and C <sub>2</sub> H <sub>5</sub> OH	200	100–200	–	≈3min	≈5–6 min	82
Li <sub>0.5</sub> Sm <sub>x</sub> Fe <sub>2</sub> O <sub>4</sub>	Sol-gel self-combustion	850 °C	850 °C	25 °C	<40%	LPG and NH <sub>3</sub>	200	–	0.2–0.15 μm	3min	5–6 min	82
Li-CuFe <sub>2</sub> O <sub>4</sub>	Co-precipitation	900 °C	900 °C	340–355 °C	83.82%	C <sub>2</sub> H <sub>5</sub> OH, methanol	0.5–4 vol%	17	7–17	2.7 min	19.36 min	159
Mg <sub>0.5</sub> Zn <sub>0.5</sub> Fe <sub>2</sub> O <sub>4</sub>	Wet chemical	750 °C	750 °C	375 °C	≈60%	Acetone	50	≈23	≈58	32 s	2–3 min	189
Mg <sub>0.5</sub> Zn <sub>0.5</sub> Fe <sub>2</sub> O <sub>4</sub>	Wet chemical	750 °C	750 °C	350 °C	≈39%	C <sub>2</sub> H <sub>5</sub> OH	50	≈23	≈58	24 s	1 min	189
Mg <sub>1-x</sub> Li <sub>x</sub> Fe <sub>2</sub> O <sub>4</sub>	Solid state reaction	300 °C	300 °C	200 °C	–	Humidity	10–80%	–	110–200	180–360 s	435–780s	214
Mg <sub>1-x</sub> Zn <sub>x</sub> Fe <sub>2</sub> O <sub>4</sub>	Wet-chemical	300–900 °C	300–900 °C	320 for CO and 380 °C for H <sub>2</sub>	44% for CO and 65% for H <sub>2</sub>	CO and H <sub>2</sub>	1660	11	–	–	–	188
MgFe <sub>2</sub> O <sub>4</sub>	Sol-gel autocombustion	1173 K	1173 K	250 °C	71%	LPG	200	–	30–38	–	–	116
MgFe <sub>2</sub> O <sub>4</sub>	Co-precipitation	900 °C	900 °C	335 °C	3.0	Petrol	5	40	1 μm	–	–	125
MgFe <sub>2</sub> O <sub>4</sub>	Solid state reaction	700 °C	700 °C	275 °C	–	C <sub>2</sub> H <sub>5</sub> OH	10–1000	–	15–30	–	–	214
MgFe <sub>2</sub> O <sub>4</sub>	Sol-gel auto-combustion	450–500 °C	450–500 °C	598 K	73%	C <sub>2</sub> H <sub>5</sub> OH	5	–	15–20	–	–	211
MgFe <sub>2-x</sub> Ce <sub>x</sub> O <sub>4</sub>	Sol-gel autocombustion	973K and 1173 K	973K and 1173 K	25 °C	50%	CH <sub>3</sub> OH	100–300	28–34	0.07–0.2 μm	20 s	65 s	212
Mn <sub>0.2</sub> Ni <sub>0.8</sub> Fe <sub>2</sub> O <sub>4</sub>	hydrothermal	–	–	250 °C	0.99	Acetone	1000–8000	27	–	450 s	90 s	217
MnFe <sub>2</sub> O <sub>4</sub>	Chemical Co-precipitate	–	–	–	93.6%	Humidity	–	10.7	–	1 s	5 min	215
MnFe <sub>2</sub> O <sub>4</sub>	Solution assisted combustion	–	–	300 K	80.6%	SO <sub>2</sub>	–	–	–	–	–	–
Ni <sub>1-x</sub> Co <sub>x</sub> Fe <sub>2</sub> O <sub>4</sub>	Spin coating	800 °C	800 °C	260 °C	83.5	NH <sub>3</sub>	–	–	30–35	–	–	216
Ni <sub>1-x</sub> Co <sub>x</sub> Mn <sub>x</sub> Fe <sub>2-x</sub> O <sub>4</sub>	hydrazine	500 °C	500 °C	180 °C	70%	C <sub>2</sub> H <sub>5</sub> OH	150	20–29	–	–	10 min	79
Ni <sub>1-x</sub> Zn <sub>x</sub> Fe <sub>2</sub> O <sub>4</sub>	Sol-gel self-auto-combustion	880 °C	880 °C	275 °C	60%	LPG	1000	10–15	–	<1 min	–	80
NiFe <sub>2</sub> O <sub>4</sub>	Co-precipitate	400 °C	400 °C	300 °C	–	Acetone	500	–	–	–	–	46
NiFe <sub>2</sub> O <sub>4</sub>	Sol-gel self-auto-combustion	600 °C	600 °C	350 °C	96%	Cl <sub>2</sub>	1000	8.36	–	12 min	–	51
NiFe <sub>2</sub> O <sub>4</sub>	Sol-gel self-auto-combustion	600 °C	600 °C	300 °C	–	C <sub>2</sub> H <sub>5</sub> OH	50	23	–	88 s	220 s	1
NiFe <sub>2</sub> O <sub>4</sub>	Sol-gel self-auto-combustion	600 °C	600 °C	230 °C	≈88%	Acetone	200	–	15–25	–	–	155
NiFe <sub>2</sub> O <sub>4</sub>	Hydrothermal	–	–	Room temperature	≈76%	Alcohol	200	–	–	–	–	–
NiFe <sub>2</sub> O <sub>4</sub>	Hydrothermal	–	–	Room temperature	–	LPG	–	8.9–11.3	12.3–14.7	–	–	80

(Continued)

Table 1. Continued.

Ferrites	Synthesized methods	Temperature Calcination	Operating	Sensitivity	Selectivity	Concentration (ppm)	Crystallite size (nm)	Particle size (nm)	Response time	Recovery time	References
NiFe <sub>2</sub> O <sub>4</sub>	Sol-gel self-auto-combustion	550 °C	350 °C	2.1	LPG	2000	23	11	≈70	≈180	72
NiFe <sub>2</sub> O <sub>4</sub>	Glycine combustion route	500 °C and 700 °C		142%	LPG	200	31 and 38	—	—	—	121
NiFe <sub>2</sub> O <sub>4</sub>	Co-precipitate	400 °C	—	62.3	LPG	4 vol %	—	—	220 s	250 s	147
PANI-CdFe <sub>2</sub> O <sub>4</sub>	Chemical polymerization	300 °C	—	50.83	LPG	1000	24	—	50 s	100 s	208
Pd-MgFe <sub>2</sub> O <sub>4</sub>	Molten salt	700 °C	—	60%	LPG	200	15–20	—	5 s	5 min	213
Sn <sub>0.2</sub> Ni <sub>0.8</sub> Fe <sub>2</sub> O <sub>4</sub>	Co-precipitate	900 °C	25 °C	68.43%	Sulfur hexafluoride	80	39	34.5–35.01	3.76s	23.21 s	204
Zn <sub>1-x</sub> Cu <sub>x</sub> Fe <sub>2</sub> O <sub>4</sub>	Sol-gel auto-combustion	630 °C	250 °C	53.35%	LPG	0.6 vol %	28–47	—	6.25 min	3.5 min	192
ZnFe <sub>2</sub> O <sub>4</sub>	Molten salt route	700 °C	250 °C	300 for H <sub>2</sub> S and rest <60	H <sub>2</sub> S, NO <sub>2</sub> , SO <sub>2</sub> , C <sub>2</sub> H <sub>5</sub> OH and acetone	200	15–20	16	3 s	<3 min	182
ZnFe <sub>2</sub> O <sub>4</sub>	Sol-gel self-autocombustion	1000 °C	350 °C	90%	C <sub>2</sub> H <sub>5</sub> OH, LPG and acetone	150	100	—	2 min	4 min	100
ZnFe <sub>2</sub> O <sub>4</sub>	Sol-gel self-autocombustion	500 °C	25 °C	140%	LPG	2000	10	30–40	60 s	300 s	48
ZnFe <sub>2</sub> O <sub>4</sub>	Ultrasonic spray pyrolysis	—	280 °C	10	CO	500	—	200	—	—	120
ZnFe <sub>2</sub> O <sub>4</sub>	Auto-combustion	560 °C	250 °C	—	C <sub>2</sub> H <sub>5</sub> OH	200–800	—	10	70 s	90 s	185
Zn <sub>0.9</sub> Mn <sub>0.1</sub> Fe <sub>2</sub> O <sub>4</sub>	Sol-gel self-autocombustion	550 °C	300 °C	—	C <sub>2</sub> H <sub>5</sub> OH	200	—	30–35	—	—	93

size, when compared with NiFe<sub>2</sub>O<sub>4</sub>, ZnFe<sub>2</sub>O<sub>4</sub>, MgFe<sub>2</sub>O<sub>4</sub>, ZnAl<sub>2</sub>O<sub>4</sub>, CoAl<sub>2</sub>O<sub>4</sub> and MgAl<sub>2</sub>O<sub>4</sub>.<sup>1</sup> Other studies support that open pores and smaller grain sizes enhance gas sensitivity.<sup>47,72</sup>

#### 2.4. Operating temperature

The measurement of gas response shown that it depended on the operating temperature.<sup>25</sup> Electrical properties of ferrites are temperature dependent<sup>73–76</sup> and are attributed by polarizations which are: interfacial, dipolar, atomic and electronic. The interfacial and dipolar polarizations, are strongly temperature dependent.<sup>77</sup> In turn therefore operating temperature determines ceramic gas sensor sensitivity. At low temperatures the gas analyte do not have enough thermal energy to react with the adsorbed oxygen species O<sub>2</sub><sup>-</sup> and hence low sensitivity. Sensitivity therefore is directly proportional to operating temperature and reaches maximum at a particular temperature.<sup>66</sup> The temperature corresponding to maximum sensitivity depend on the type of the test gas, chemical composition, dopants as well as catalyst.

The enhanced sensitivity at elevated temperature is attributed by enough high thermal energy which help to overcome the activation energy barrier of the surface reaction and as well as the conversion of adsorbed oxygen species from O<sub>2</sub><sup>-</sup> to O<sup>-</sup> at increased temperatures increasing electron concentration resulting from the sensing reaction of a target gas and O<sup>-</sup> upon the maximum sensitivity is attained. Further increase of temperature leads to a higher desorption as compared to the adsorption rate since high temperatures are not favorable to the exothermic adsorption process and hence the sensitivity response declines.<sup>66</sup> Tudorache et al.<sup>78</sup> showed maximum sensitivities of CdFe<sub>2</sub>O<sub>4</sub> and ZnFe<sub>2</sub>O<sub>4</sub> as LPG, ethanol and acetone sensor at 350 °C while CuFe<sub>2</sub>O<sub>4</sub> at 300 °C and NiFe<sub>2</sub>O<sub>4</sub> at 250 °C. Kapse<sup>1</sup> showed maximum sensitivity of MgFe<sub>2</sub>O<sub>4</sub> LPG sensor at 325 °C and for NiFe<sub>2</sub>O<sub>4</sub> at 300 °C. Satyanarayana et al.<sup>79</sup> showed that sensitivity of NiFe<sub>2</sub>O<sub>4</sub> toward LPG increased with temperature and reached maximum sensitivity at 250 °C. Rezlescu et al.<sup>65</sup> showed that maximum sensitivity of CdFe<sub>2</sub>O<sub>4</sub> and ZnFe<sub>2</sub>O<sub>4</sub> appeared at 300 °C all used as LPG, ethanol and acetone sensors. Generally, ferrites sensors require thermal activation for the redox reaction to occur.

## 2.5. Sensitivity

Sensitivity can be defined as the ration in Eq. (5),<sup>80</sup> where,  $R_g$  is sensor resistance in the presence of test gas analyte and  $R_a$  is the sensor resistance in the presence of air.

$$S = \frac{R_a}{R_g} \text{ sensitivity for reducing gas or}$$

$$S = \frac{R_g}{R_a} \text{ for oxidizing gas} \quad (5)$$

It can also refer as the ratio of the change of resistance in test gas analyte to value of resistance in air, Eq. (6).

$$S(\%) = \frac{(R_a - R_g)}{R_g} \times 100 \quad (6)$$

It is dependent of concentration of gas (more often a direct relationship)<sup>81,82</sup> as well as the type of ferrite.<sup>83,84</sup> The sensor resistance rises in an oxidizing gas analyte while on the other hand it decreases in a reducing gas analyte. Sensitivity also depends on the pore size, porosity and specific area. Large specific surface result in high sensitivity within certain limits. In the production of ferrite sensor, the control of these parameters is a major problem. These problems are solved by suitable sintering temperature and introduction of suitable additives that stimulate the pore formation. Gas sensitivity tends to saturate in the range of high concentration.<sup>85</sup> Patil et al.<sup>11</sup> showed sensitivity of  $\alpha$ -Fe<sub>2</sub>O<sub>4</sub> toward LPG increased as concentration increased stepwise from 5–60 ppm. Rezlescu et al.<sup>65</sup> showed sensitivity of ZnFe<sub>2</sub>O<sub>4</sub> LPG sensor increased as concentration increased from 0–150 ppm. Sensitivity depends on the depletion layer width for semiconductor ferrites.<sup>47</sup>

## 2.6. Selectivity

The sensor capability to selectively detect a particular gas analyte in the presence of other gases is referred to as its selectivity.<sup>86</sup> It is an important parameter since in practical application environments, gases would exist as a mixture. Both sensitivity and selectivity are improved by temperature control,<sup>87</sup> use of catalyst and dopants,<sup>66,88</sup> special additives to the surface of the grain as well as the application of filters. Selectivity can also be enhanced by appropriate thickness of sensing layer as well as electrode configuration.<sup>89</sup> Different ferrites have different selectivity to various gases. Rezlescu et al.<sup>81</sup> showed selectivity of CuFe<sub>2</sub>O<sub>4</sub>, CdFe<sub>2</sub>O<sub>4</sub> and ZnFe<sub>2</sub>O<sub>4</sub> toward LPG, ethanol

and acetone. Poghossian et al.<sup>85</sup> showed selectivity of BiFe<sub>2</sub>O<sub>3</sub> toward acetone. Singh et al.<sup>90</sup> showed selectivity of SrFe<sub>12</sub>O<sub>19</sub> toward LPG. Kamble et al.<sup>51</sup> showed selectivity of NiFe<sub>2</sub>O<sub>4</sub> toward Cl<sub>2</sub>. Generally selectivity of various ferrites sensors to various gases differs that is some ferrites can detect various gases while others not.

## 2.7. Dopants (influence to sensitivity, selectivity and operational temperature)

Ferrite gas sensor sensitivity, selectivity and response time can be improved by adding or substituting metal ions in ferrites e.g. Sutka et al.<sup>47</sup> found that due to increase of donor concentration the overall sensitivity increases which is attributed by increased adsorbed oxygen species on the grain surface. Joshi et al.<sup>55</sup> studied induced effect on CO and ethanol sensing properties of cobalt ferrite nanoparticles. Improved sensitivity was observed and working temperature reduced from 325 °C to 225 °C. Kadu et al.<sup>91</sup> examined the incorporation of palladium influenced Zn<sub>0.6</sub>Mn<sub>0.4</sub>Fe<sub>2</sub>O<sub>4</sub> ethanol sensor. It was showed that sensitivity increased and the operating temperature reduced from 300 °C to 200 °C. Pathania et al.<sup>92</sup> examined the effect of tungsten substituted nickel ferrite toward hydrogen. The sensor showed improved sensitivity at a minimum temperature of 80 °C. Gadkari et al.<sup>93</sup> studied the effect of sm<sup>3+</sup> ion addition on sensing properties of MgCd<sub>x</sub>Fe<sub>2</sub>O<sub>4</sub> toward LPG, Cl<sub>2</sub> and C<sub>2</sub>H<sub>2</sub>OH. It was observed that working temperature lowered to 198 °C from 222 °C. As it have been shown by the above examples, the main role of metal substitution in ferrite gas sensors is to lower the operating temperature and increasing sensitivity as well. This is achieved by two ways; first is by the change of microstructure of ferrite by reducing the particle size which provides a higher surface area. Secondly, substitution modifies the electrical conductivity of the ferrite which enhances sensitivity.

## 2.8. Response characteristics

To quote Reddy et al.,<sup>94</sup> 'the response characteristics give an idea of the rise time, i.e. the time taken by the sensor to respond to the presence of a gas and the fall time, i.e. the time taken by the sensor to come back to its original value once the test gas is removed'. It is also the resistance to the time relationship in gas concentration changes and the change in resistance which is made from atmosphere of fixed concentration of the test gas to clean air, at a fixed temperature and



gas concentration.<sup>53</sup> Korotcenkov<sup>95</sup> defined response time as the period from the time when the gas concentration reaches a specific value to that when the sensor generate a corresponding signal. Mostly, it is considered as the time taken to reach 90% of the highest sensing response.<sup>96</sup> Response characteristics i.e. recovery times and response times, are dependent on the gas adsorption, humidity presence and thus water molecule desorption<sup>96,97</sup> bulk nature of the sensor element,<sup>2</sup> rate of diffusion of the gas vapor through the sensor microspores,<sup>98</sup> working temperature, gas type<sup>25,99</sup> and gas concentration.<sup>100</sup>

### 2.9. Sensor resistance to gas concentration

This parameter shows effect of gas concentration ( $C_g$ ) toward conductivity ( $G_s$ ) or sensor resistance  $R_s$ .<sup>53</sup> The parameter depends on temperature, gas concentration and has first sensor resistance in air ( $R_a$ ) that transient to its constant state value ( $R_{ag}$ ) during sensing of the gas.<sup>101</sup> At low concentration of the gas in air atmosphere in a particular constant temperature the conductivity is given by Eq. (7).<sup>102</sup>

$$G_s = KC_g^\alpha \quad (7)$$

where  $K$  and  $\alpha$  are constants and  $C_g$  is the gas concentration parameter in air.

### 2.10. Fabrication and morphology of gas sensor

The oxygen chemisorption centers i.e. localized donor or acceptor states, oxygen vacancies as well as other defects are formed on the surface during fabrication process of the material.<sup>56,103</sup> Thus fabrication and the morphology of a sensor is an important parameter in gas sensing. Ferrite sensors can be made as thick film,<sup>51</sup> pellet form,<sup>56</sup> thin film,<sup>2</sup> nanorods<sup>104,105</sup> and nanocubes.<sup>59,106</sup> They consists of large grained or nanocrystalline material employing different technologies such as physical vapor deposition (PVD),<sup>107</sup> chemical vapor deposition (CVD),<sup>108</sup> drop coating process,<sup>109</sup> sputtering.<sup>110</sup> Some of these materials are effective due to their reproducibility in fabrication, less expensive as well as faster response to gases. The size of the sensor shrink to about 1 mm × 1 mm in thick films and therefore achieve low power consumption. In the case of thick film the sensors are prepared through screen printing method where the paste is made by mixing chemically sensitive powder with an organic binder such as poly-vinyl alcohol (PVA)<sup>111</sup> or  $\alpha$ -terpineol.<sup>1</sup> The pastes are coated on substrates for example alumina tube and ceramic tubes. In bulk

type, many ferrite sensors are produced by convective ceramic sintering process having either cylindrical shape or rectangular shape.<sup>85</sup> They are operated at temperature ranging from 300 °C to 500 °C. They are widely used for toxic, reducing as well as inflammable gases because of their long term stability contributed by their structural properties.

### 2.11. Phase formation

Ferrites are ceramics and exist in different controllable phases, and phase formation is dependent on the composition and sintering temperature.<sup>112</sup> The lower phase formation temperature limits the growth of crystal favoring ferrites in the gas sensing application.<sup>113,114</sup> In the case where ferrite consist of many phases, its properties depend on each phase properties separately and the way these phases occur on aggregates. Mukherjee et al.<sup>115</sup> showed that the phase purity, larger surface area, smaller particle size as well as mesoporous surface morphologies of  $Mg_{0.5}Zn_{0.5}Fe_2O_4$  ferrite particles have enhanced effect on the gas sensing performances.

### 2.12. Surface phenomena and gas sensing mechanism

#### 2.12.1. Adsorption

The adsorption of oxygen on a material surface is a function of the specific area and its intrinsic properties, and the response of a material to the reducing gases is a function of the amount absorbed.<sup>116</sup> Adsorption is the process whereby the solid or liquid surface is accumulated with either gas or liquid solute forming a film of molecules or atoms. On the other hand absorption refers to a chemical or physical process whereby either molecules, ions or atoms enter some bulk phase gas solid or liquid material. Adsorption can also refer to the process by which molecules or particles are binded to the surface. The term sorption applies for both absorption and adsorption.<sup>117</sup> There are two types of adsorption; physical and chemical adsorption.<sup>118</sup> In physical adsorption may it be atoms or molecules they maintain their individuality with electrostatic forces of interaction within the surfaces. Both physical adsorption and desorption mainly occur at low temperature as a result of low binding energy to the surface. The interacting forces are caused by van-der wall forces which originates from mutually induced dipoles moments. On the other hand in chemisorption the atoms or molecules are bonded by covalent bond and partially

ionic with the crystal. Contrary to physical adsorption chemisorption takes place at higher temperature as a result of high binding energy which is above 1 eV.<sup>102</sup> Under suitable condition physisorption gas phase molecule forms multilayer adsorption while in chemisorption only monolayer adsorption forms due to the molecules being adsorbed on the surface by valence bond. In both adsorptions the adsorbed molecules or atoms form donor or receptor surface levels.

### 2.12.2. Surface state

Gas sensing at low concentrations is dependent of the surface state.<sup>87,119</sup> Surface state is localized states energy levels at the materials surface. In ionic crystal materials for examples semiconducting metal oxide surface states are grouped in to as intrinsic and extrinsic states.<sup>120</sup> Intrinsic results from the lattice distortion periodicity at the surface. On the other hand extrinsic states come from adsorption of impurities and gases on the surface.

### 2.12.3. Mechanism of gas sensing

The mechanism of gas sensing is a major parameter. In this review, we discuss the mechanism in § 3.

## 3. Gas sensing mechanism in ferrites

Spinel ferrites gas sensors work in a similar manner as semiconductor gas sensor,<sup>121,122</sup> in other words the sensing mechanism is electrical conductance related.<sup>76,123,124</sup> Electrons are trapped by O<sub>2</sub> species chemisorbed onto the metal oxide particles as shown in Figure 2.<sup>2</sup> This leads to the formation of a resistance layer as a result of electron depleted on the space charge on the n-type particle surface or the conducting layer which results from accumulated holes on the p-type particles, see Figure 3.<sup>125</sup>

Oxide sensor works under the principle of change in the capacitance or electrical resistance as a result of the adsorption of gases.<sup>53</sup> The change in electrical resistance is a function of test gas analyte which is the major mechanism of sensing of the surface conductive gas sensor.<sup>120</sup> Upon the exposure of reducing for example CO, CO react with adsorbed O<sup>-</sup> thereby releasing the trapped electron to the conduction band and hence the resistance lower. In ferrite, the mechanism of sensing is based on the surface controlled process.<sup>126</sup> The process is described by two process i.e. adsorption and ionization of oxygen from air containing the test gas analyte as shown by the following expression

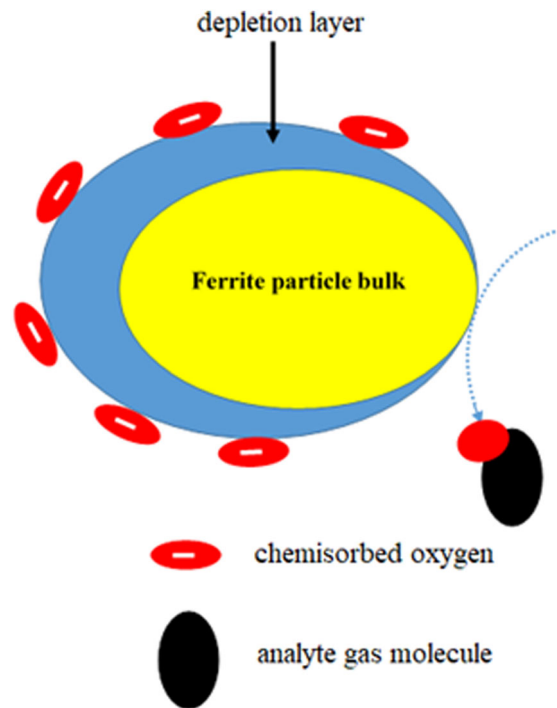
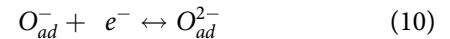
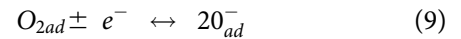


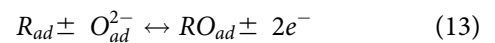
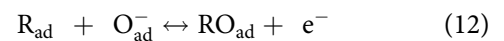
**Figure 2.** Gas sensing mechanism showing the formation of depletion region in a ferrite particle due to chemisorbed oxygen. Upon the exposure to an analyte gas, the gas react with adsorbed O<sup>-</sup> thereby releasing the trapped electron to the conduction band and hence the resistance lower.



where “gas” and “ad” shows the gaseous and oxygen adsorbed respectively. For reducing gases (R) it can be absorbed on the sensor material surface as by expression (11).



The reaction of the gas adsorbed and the oxygen species adsorbed such as O<sub>ad</sub><sup>-</sup> and O<sub>ad</sub><sup>2-</sup> then they proceed as shown in Eqs. (12) and (13).



At the end of the desorption takes place as per expression 2.9 c.<sup>116</sup>



The sensing property of various gases results from difference in the reaction and the adsorption processes. Adsorbed oxygen species play a key role in that it provides enough reactant for the reaction.<sup>127</sup> In order to improve sensing properties catalytically active compounds are added.<sup>126</sup>

### 3.1. P-type spinel ferrite gas sensors

P-type inverse spinel structure has transition  $M^{2+}$  cations in the octahedral site besides  $Fe^{2+}$ .<sup>47</sup> The p-type conductivity results from the hopping holes between octahedral sites. Darsane et al.<sup>99</sup> examined gas sensing

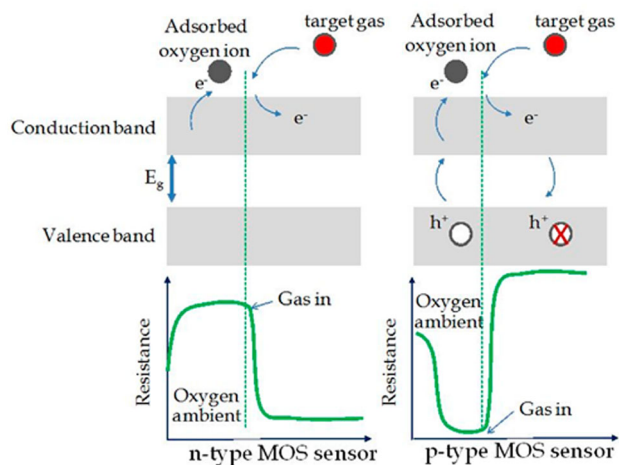


**Figure 3.** Schematic diagram for change of the sensor resistance upon exposure to the target gas (reducing gas) in the cases of n-type and p-type metal oxide sensors. Figure obtained from Fazio et al.<sup>125</sup>

mechanism of  $NiFe_2O_4$  toward LPG p-type conductivity was observed which resulted from hole hopping  $Ni^{3+}$  in octahedral site. Kadu et al.<sup>91</sup> examined  $Co_{1-x}NiFe_2O_4$  as CO and ethanol sensor. P-type conductivity was observed in the pure cobalt ferrite as a result of the hopping holes between  $Co^{3+}$  and  $Co^{2+}$  ion pair in the octahedral site. In the presence of reducing gases for examples CO,  $CH_4$ , and LPG the sensor resistance increases.<sup>85</sup> Kim et al.<sup>128</sup> examined  $Bi_2Fe_2O_4$  as ethanol acetone and natural gas sensor. The sensor showed increase in resistance. On the other hand, in the presence of the oxidizing gases the electrical resistance of the p-type sensor is reduced. The decrease in conductivity is due to the electron recombination with the hole.<sup>47</sup>

### 3.2. N-type spinel ferrite gas sensors

This are gas sensors which the transport charge carriers are provide by hopping electrons iron cations sited in octahedral sites.<sup>47</sup> The sensor are lowered from their chemical composition and before oxygen chemisorption cations  $Fe^{2+}$  and  $Fe^{3+}$  pair in the octahedral locations. Satyanarayana et al.<sup>79</sup> examined the

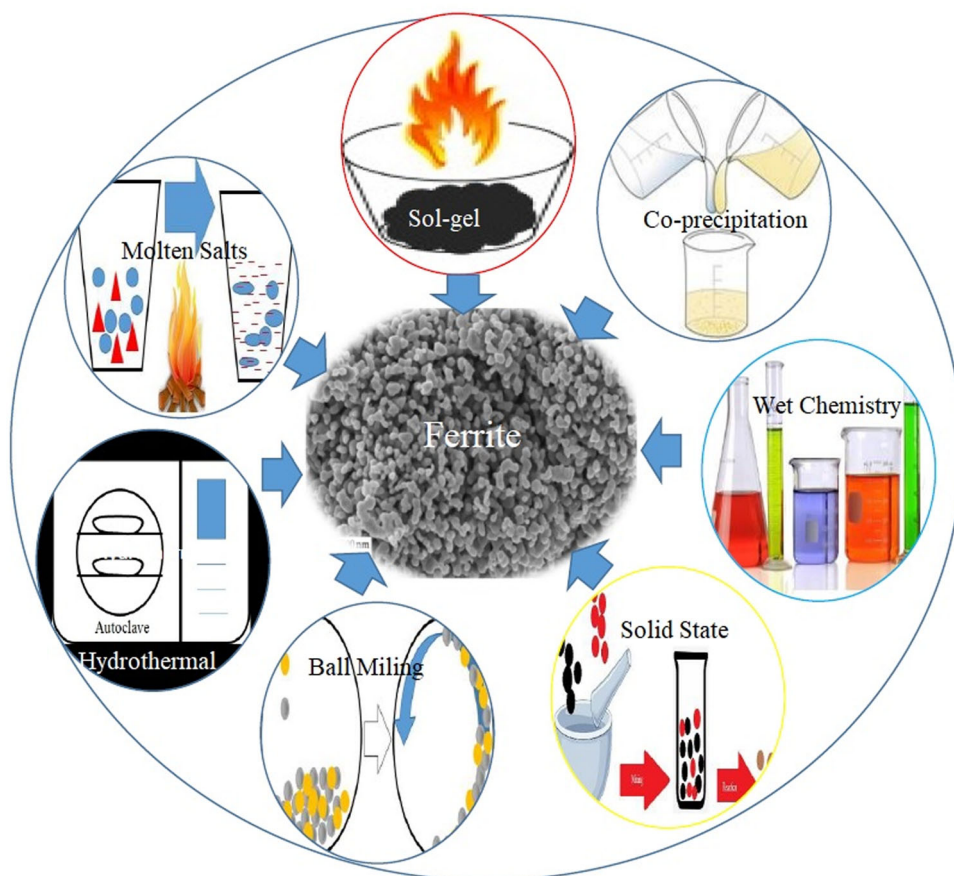


**Figure 4.** Metal ferrites synthesis method.

sensing mechanism of  $\text{NiFe}_2\text{O}_4$  sensor toward LPG. The sensor possessed n-type conductivity. Rezlescu et al.<sup>98</sup> studied the sensing mechanism of  $\text{CdFe}_2\text{O}_4$ ,  $\text{CuFe}_2\text{O}_4$  and  $\text{ZnFe}_2\text{O}_4$  toward LPG and acetone. It was observed that during the reduction process, free electrons into the semiconductors ferrites which increased gas response. Gadkari et al.<sup>93</sup> examined  $\text{Mg}_{1-x}\text{Cd}_x\text{Fe}_2\text{O}_4$  sensing mechanism toward LPG, chlorine and ethanol. On the exposure to LPG the concentration of the electron on the surface increased which resulted to increased conduction band electron. Due to the increase in electrons, the electrical resistance decreased hence sensitivity increased. Mukherjee et al.<sup>129</sup> examined sensing mechanism of  $\text{MgFe}_2\text{O}_4$  toward hydrogen and carbon monoxide. N-type conductivity was observed in which free electrons were generated into the semiconductors ferrite thereby increasing gas response. Generally, on the exposure to reducing gases the gas response or conductivity of the sensor increases.<sup>80</sup>  $\text{BiFe}_2\text{O}_3$  as ethanol and acetone sensor showed increased conductivity indicating n-type conductivity.<sup>85</sup>

### 3.3. Substituted and mixed ferrites sensors

Substituted ferrites consist of more than two different cations. The main role of metal substitution in ferrite gas sensors is to lower the operation temperature as well as increasing the sensitivity.<sup>91</sup> The improved sensitivity in metal substitution changes or modifies the properties of ferrites such as electrical properties<sup>130,131</sup> substituted  $\text{Ni}^{2+}$  by  $\text{Zn}^{2+}$  in  $\text{NiFe}_2\text{O}_4$  and studied Sensing toward acetone. The substitution strongly affected its electronic structure. It was shown that the resistivity of  $\text{Ni}_{1-x}\text{Zn}_x\text{Fe}_2\text{O}_4$  nano-sized particles increased as  $\text{Zn}^{2+}$  increased and the conductivity type changes from p-type to n-type. Jiang et al.<sup>132</sup> studied the effect of vanadium addition to  $\text{ZnFe}_2\text{O}_4$  as ethanol benzene and acetone sensor. It was found that on vanadium ( $\text{V}^{5+}$ ) substitution, there was a decrease response toward ethanol and acetone but increase to benzene. This was as result of catalytic oxidation behavior of vanadium. Sutka et al.<sup>133</sup> examined the effect of substituting  $\text{Co}^{2+}$  for  $\text{Ni}^{2+}$  in  $\text{NiFe}_2\text{O}_4$  sensor. It was found that gas response lowered. This was as a result of preferred octahedral sites and as a result, resistivity increased in inhibiting the transfer of holes between  $\text{Ni}^{2+}$  and  $\text{Ni}^{3+}$ . Mukherjee et al.<sup>13</sup> investigated the sensing mechanism of Mg-Zn ferrite. The sensor was observed to have n-type conductivity. As the sensor was introduced in the presence of reducing gases for example CO, it reacted with the chemisorbed oxygen species which resulted to lowered potential

barrier which resulted to decrease in resistance. This reduction in resistance enhanced sensitivity. Sharma<sup>134</sup> investigated the sensing mechanism of nickel substituted Mg-Zn ferrite. It was found that  $\text{Ni}^{2+}$  occupied octahedral sites where they were oxidized upon the exposure to the test gas thus changing the electrical resistance of the material. As per the above example it has been shown that substituted ferrites exhibit a change in response of the gas, but the change in direction is not always predictable.

### 3.4. Spinel ferrite humidity sensor

Spinel ferrites consists of water vapor dissociation active sites and therefore used for sensing water.<sup>130</sup> They show long lifetime as well as better sensitivity reversibility. The mechanism of humidity sensing can be explained in two steps. At first chemisorbed water displaces oxygen forming  $-\text{OH}$  groups monolayer.<sup>135</sup> Afterwards, water molecules are physisorbed leading to dissociating as a result of high electrical fields which are in the chemisorbed layers. Electrolytic conductivity becomes dormant at high humidity levels.<sup>136</sup> Morphology just like other ferrite sensors, affects sensitivity of humidity sensors. High specific surface area favors water adsorption. Small pores of about 3–50 nm adsorbs water molecules condensing it by capillary action. This lowers electrical resistivity due to electrolytic conduction.<sup>137</sup> Shah et al.<sup>138</sup> examined magnesium ferrite sensing toward humidity. It was found that on exposure the conductivity of the sensor increased due to physisorption of water vapor. The conductivity was a result of hopping  $\text{H}^+$  ions through water. Response of humidity sensors can be improved by replacing ferrites with the foreign elements. Shah et al.<sup>139</sup> showed cerium oxide incorporation in  $\text{MgFe}_2\text{O}_4$  created more oxygen vacancies which lead to a bigger number of appropriate water adsorption sites. Shah et al.<sup>139</sup> showed that Pr incorporation in  $\text{MgFe}_2\text{O}_4$  increased the reaction which have high electronegative  $\text{OH}^-$ . This increased the sensor response. Generally, mixed, substituted and doped ferrites provide promising materials for developing humidity gas sensors due to their magnetic and electrical characteristic.

## 4. Ferrite gas sensors

This section discusses various metal ferrites that have been studied as gas sensors. A summary is presented in Table 1.

## 4.1. Nickel ferrite and nickel doped ferrite

### 4.1.1. Nickel ferrites

Nickel ferrite is one of the most studied (see Table 1), as a gas sensor to sense a wide range of gases such as, LPG;<sup>51,90,99,119,140–142</sup> acetone,<sup>47,119,143,144</sup> ethanol,<sup>47,119</sup> ammonia,<sup>51,144,145</sup> Acetone,<sup>98,140,146,147</sup> ethanol,<sup>140,144,146</sup> methane (CH<sub>4</sub>),<sup>140,141,144,146</sup> Oxygen (O<sub>2</sub>),<sup>51</sup> Chlorine (Cl<sub>2</sub>),<sup>51,148</sup> trimethylamine,<sup>149</sup> toluene,<sup>47,144</sup> carbon monoxide (CO),<sup>141,144</sup> Carbon dioxide (CO<sub>2</sub>),<sup>90</sup> butane (C<sub>4</sub>H<sub>10</sub>),<sup>141</sup> hydrogen gas (H<sub>2</sub>)<sup>144,150</sup> and Heptane,<sup>47</sup> hydrogen sulfide (H<sub>2</sub>S)<sup>150</sup> as well as humidity.<sup>141,142</sup>

Kamble et al.<sup>51</sup> examined gas sensing properties of NiFe<sub>2</sub>O<sub>4</sub> thick films where nanocrystalline was synthesized by chemical co-precipitate and thick film prepared by screen printing technique. The dried powders were sintered at a temperature of 400 °C for 8 h. From XRD the crystallite size calculated by Scherer's equation was found to be 8.36 nm. Maximum sensitivity of 96% toward 1000 ppm of Cl<sub>2</sub> at 60 °C and at response time of 12 min was observed. Ghosh et al.<sup>150</sup> studied acetone and alcohol sensitivity of nanocrystalline NiFe<sub>2</sub>O<sub>4</sub> prepared through sol-gel combustion method. From TEM images regular-shaped aggregates were formed by aggregation of very fine particles sizes ranging from 15–20 nm. Sensitivity increased with operating temperature before reaching saturation at optimal temperature. Highest sensitivity of ≈88% was observed in the exposure to 200 ppm of acetone at 350 °C while sensitivity of ≈76% was observed for 200 ppm of alcohol at 300 °C. Satyanarayana et al.<sup>79</sup> studied LPG sensing properties of NiFe<sub>2</sub>O<sub>4</sub> synthesized by hydrothermal method. XRD analysis confirmed that ferrite exhibited spinel cubic structure. The size of the crystals was found in the range of 8.9–11.3 nm while the size of the particle was found to be in the range of 12.3–14.7 nm. It was found that sensitivity increased with temperature up-to saturation point at 230 °C.

Kapse<sup>1</sup> examined the H<sub>2</sub>S, NH<sub>3</sub>, C<sub>2</sub>H<sub>5</sub>OH and LPG sensing characteristics of NiFe<sub>2</sub>O<sub>4</sub> synthesized by citrated sol-gel route. The study obtained powder was sintered at 600 °C for 5 h. XRD showed that ferrite exhibited single phase spinel structure and the size of the crystallite calculated using Debye-Scherrer's formula was determined to be ≈23 nm. Maximum sensitivities of 2.1, 0.6, 6.4 and 2.7 at 300 °C were obtained for H<sub>2</sub>S, NH<sub>3</sub>, C<sub>2</sub>H<sub>5</sub>OH and LPG respectively all at a concentration of 50 ppm. For the case of C<sub>2</sub>H<sub>5</sub>OH both response time as well as recovery time were observed at 88 s and 220 s respectively. Singh et al.<sup>90</sup> studied LPG sensing characteristics of nanocrystalline NiFe<sub>2</sub>O<sub>4</sub> thin films prepared through sol-gel auto-

combustion technique. Fabricated films were heat treated at 500 °C for 3 h to enhance ceramic properties. From SEM and XRD analysis, the specific surface area of NiFe<sub>2</sub>O<sub>4</sub> was found to be 57 m<sup>2</sup>/g, crystallite size of 23 nm and most dispersed particles were found to be 11 nm. At a room temperature the sensitivity of 2.1 which had response time and recovery time of ≈70 s and 180 s respectively were observed toward 200 ppm of LPG.

Patil et al.<sup>119</sup> examined LPG, acetone, C<sub>2</sub>H<sub>5</sub>OH and NH<sub>3</sub> sensing characteristic of NiFe<sub>2</sub>O<sub>4</sub> prepared through glycine combustion method. The powders were sintered at 500 °C and 700 °C. XRD confirmed formation of cubic spinel structure ferrites with crystallite size averaging to 31 nm for powder calcined at 500 °C and 38 nm for calcined at 700 °C. It was observed that the sensor had highest sensitivity and selectivity toward LPG. Maximum response of 142% at 350 °C was observed toward 200 ppm of LPG. Generally for all test gases it was observed that gas response increased linearly with concentration. Liu et al.<sup>141</sup> synthesized NiFe<sub>2</sub>O<sub>4</sub> by co-precipitate route and studied its LPG and humidity sensing properties. The obtained powder was calcined at 400 °C for 2 h. From XRD analysis the crystallite size was observed to be in the range of 15–50 nm. SEM micrographs showed more pores which gave largest effective surface area. The average sizes of the pore of samples were observed to be in the range of 1.2 μm–2.5 μm. It was found that sensitivity linearly depended with concentration up-to a saturation point. Maximum sensitivity of 63.2 for 4 vol % of LPG was observed. Both response time and recovery time were observed at 220 s and 250 s respectively. Maximum sensitivity toward humidity for the range 10–90% was found to be 54 MΩ/%RH.

### 4.1.2. Nickel doped ferrites

Various studies as summarized in Table 1, has studied the influence of ion substitution in nickel ferrite e.g. by substitution with Copper,<sup>83,151</sup> Lithium,<sup>152–155</sup> Manganese,<sup>83,156,157</sup> Palladium,<sup>158</sup> Silver,<sup>159</sup> Tin,<sup>152</sup> Zinc<sup>12,81,160–162</sup> and double substitution with cobalt and Manganese,<sup>79</sup> Copper and Zinc.<sup>129</sup>

Sutka et al.<sup>47</sup> examined the effect of zinc ion to NiFe<sub>2</sub>O<sub>4</sub> sensors. The samples for Ni<sub>1-x</sub>Zn<sub>x</sub>Fe<sub>2</sub>O<sub>4</sub> (x = 0, 0.3, 0.5 and 0.7) were synthesized through sol-gel auto-combustion technique and heat treated at 800 °C. From XRD analysis cubic spinel type structure was formed for all samples. For all samples porosity was found to >60%. It was observed that the response toward 500 ppm of acetone was a function of both

operating temperature and composition. With increase in working temperature the response increased to peak and then decreased. Maximum response appeared at 275 °C. Iftimie et al.<sup>140</sup> studied acetone, C<sub>2</sub>H<sub>5</sub>OH, CH<sub>4</sub> and LPG sensing characteristics of Ni<sub>0.99</sub>Co<sub>0.01</sub>Mn<sub>0.02</sub>Fe<sub>0.02</sub>O<sub>4</sub> synthesized by self-combustion method. The powder obtained was pressed into a disk shape and then heat treated at 1000 °C for 30 min. XRD analysis confirmed spinel structure of the ferrite. SEM images showed that the samples consisted irregularly-shaped of 1–6 μm aggregates of fine 0.1 μm particles. The size of the crystallites was observed to be ranging from 100–500 nm, high intergranular porosity of 40% and bulk density of 3.11 g/cm<sup>2</sup>. Sensitivity toward acetone was observed to be best and almost insensitive to methane. Sensitivity increased linearly with operating temperature and reached maximum value at 230 °C and decreased on further increase. Jiao et al.<sup>118</sup> examined acetone sensing properties of amorphous Ag modified NiFe<sub>2</sub>O<sub>4</sub> synthesized through solid state reaction method. The samples were calcined at 800 °C. It was found that for 1.5% Ag modified NiFe<sub>2</sub>O<sub>4</sub> sensor a maximum sensitivity of 43 toward 1000 × 10<sup>6</sup> acetone vapor at steady operating voltage of 4.5 V. Both response time and recovery time were found at 1 s and 10 s respectively.

Manikandan et al.<sup>152</sup> synthesized Sn<sub>0.2</sub>Ni<sub>0.8</sub>Fe<sub>2</sub>O<sub>4</sub> by co-precipitate method and fabricated thin film sensor. Thin film sensing properties toward sulfur hexafluoride gas were studied. thin film were heat treated at 900 °C for 4 h. XRD confirmed that the structure of the sample was cubic spinel and the crystallite size calculated using Debye Scherrer formula was found in the average range of 39 nm. The size of the particle obtained from SEM was found to be in the range of 34.5–35.02. Maximum sensitivity of 68.43% toward 80 ppm of the gas was found at 25 °C. Response time and recovery time were observed at 3.76 and 23.21 min respectively.

## 4.2. Cobalt ferrite and cobalt doped ferrites

### 4.2.1. Cobalt ferrites

Cobalt ferrites are popular too in gas sensing to sense LPG,<sup>163–165</sup> nitrogen dioxide,<sup>166</sup> ammonia (NH<sub>3</sub>),<sup>163,164,167,168</sup> ethanol (C<sub>2</sub>H<sub>5</sub>OH),<sup>149,163,164</sup> sulfur dioxide (SO<sub>2</sub>),<sup>163</sup> methanol (CH<sub>3</sub>OH),<sup>166</sup> nitrogen dioxide (NO<sub>2</sub>),<sup>166</sup> hydrogen sulfide (H<sub>2</sub>S),<sup>164</sup> carbon dioxide (CO<sub>2</sub>),<sup>164</sup> hydrogen (H<sub>2</sub>)<sup>164</sup> and Chlorine (Cl<sub>2</sub>).<sup>164</sup> Bagade et al.<sup>166</sup> prepared CoFe<sub>2</sub>O<sub>4</sub> thin film through chemical spray pyrolysis and examined

nitrogen sensing properties. In enhancing physico-chemical and sensing properties, coated cobalt ferrite films were sintered at 900 °C. XRD confirmed polycrystalline nature of the film as well as spinel cubic structure. From the surface morphology it was observed that the grain structure had grain size averaged to about 200 nm–400 nm. Highest gas sensor response of 95% for 80 ppm of N<sub>2</sub> was recorded at optimum temperature of 300 °C. Response and recovery time were observed at 5 sec and 117 sec. Leroux et al.<sup>167</sup> synthesized Co<sub>x</sub>Fe<sub>3–x</sub>O<sub>4</sub> (for x ranges from 1–8) through wet chemical route and examined its sensitivity toward NH<sub>3</sub>. It was found that for each cobalt amount the powder was very homogenous in composition, size and well dispersed. The particle size decreased with cobalt amount x to <10 nm. The sensors were calcined at 175 °C for 48 h to impact gas sensing properties. Maximum sensitivity toward 25 ppm of NH<sub>3</sub> was obtained at 227 °C. Xiangfeng et al.<sup>149</sup> synthesized CoFe<sub>2</sub>O<sub>4</sub> nano-crystalline by hydrothermal method and examined its sensing property toward ethanol. XRD showed that spinel CoFe<sub>2</sub>O<sub>4</sub> was obtained in the Ph range of 8–14. From the SEM the particle size ranged from 15–20 nm with particle size increasing with hydrothermal reaction time. CoFe<sub>2</sub>O<sub>4</sub> obtained under Ph 8 portrayed the highest response of 71.9 at 150 °C of 10 ppm ethanol. Bagade et al.<sup>163</sup> studied morphological, structural, and magnetic as well as gas sensing properties of CoFe<sub>2</sub>O<sub>4</sub>. Thin film deposited on the quartz substrate by spray pyrolysis technique, films were annealed at 900 °C for 4 hour. In ambient atmosphere, XRD showed that the film formed spinel cubic structure. The size of the crystallite was observed to be in the range of 150 nm–200 nm of the samples prepared. It was found that sensitivity was a function of both working temperature and concentration of the gas. It was found that resistance increased upon exposure to NO<sub>2</sub> with response time increased from 5 s at 5 ppm to 9 s at 80 ppm. Additionally recover time also increased from 130 s to 160 s with NO<sub>2</sub> concentration at 150 °C.

### 4.2.2. Cobalt doped ferrites

Cobalt substituted ferrites perform well in sensing of the mentioned gases. Cobalt has been substituted with nickel,<sup>47,78,91,133,169</sup> with Semarium,<sup>43</sup> with manganese,<sup>83,170–172</sup> with cerium,<sup>173</sup> with manganese,<sup>83,174</sup> and doubly substituted to form a ternary ferrite of cobalt, nickel and zinc.<sup>175</sup> Bagade et al.<sup>170</sup> prepared Co<sub>1–x</sub>Mn<sub>x</sub>Fe<sub>2</sub>O<sub>4</sub> (for x ranges from 0.0–0.5) by chemical spray pyrolysis and studied its sensing characteristics toward NO<sub>2</sub> gas. It was observed from the XRD

that the film exhibited single phase inverse spinel cubic structure with the size of crystallite varying from 45 nm to 65 with relation to  $Mn^{2+}$  concentration. The film was annealed at 900 °C for 4 h in order to get better structural properties which aided gas sensing properties. Maximum gas response of 1.62 was found at working temperature of 150 °C for 100 ppm of  $NO_2$ . Maximum sensitivity recorded was at 90%. Tudorache et al.<sup>78</sup> studied  $Ni_{1-x}Co_xFe_2O_4$  ( $x=0.25, 0.5$  and  $0.75$ ) sensing properties in thin films coated on a glass substrates through spin coating technique. To obtain oxide nanocrystalline thin film the sensor was sintered at 800 °C for 1 hour. The size of the crystallites was calculated using Scherrer equation was found to increase with increase with  $x$  in the range of 20–29 nm. It was found that gas sensitivity was a function of working temperature, type and gas concentration, microstructure as well as material composition. It was found that gas sensitivity to alcohol increased from 56% to 66% as the constant in Co increased from  $x=0.25$  to  $x=0.75$  at 260 °C. Sensitivity to 150 ppm acetone increased from 49% to 61% when the constant in Co decreased from  $x=0.75$  to  $x=0.25$ . Maximum sensitivity of about 70% toward 150 ppm alcohol was obtained at 260 °C with the film having a recover time of 10 min. Kadu et al.<sup>91</sup> examined CO and  $C_2H_5OH$  sensing properties of  $CO_{1-x}Ni_xFe_2O_4$  ( $x=0, 0.5$  and  $1.0$ ) prepared through chemical co-precipitation technique. From XRD it was observed that single phase cubic spinel structure was formed by all the samples. The size of the crystallite calculated using Scherrer's equation was found to be in the range of 10–20 nm. It was found that sensitivity increased with operating temperature as well as the concentration up to a saturation point. Optimal temperature of 325 °C was attained for 1000 ppm of CO gas while for 1000 ppm of  $C_2H_5OH$  was observed at 250 °C

### 4.3. Zinc ferrites and zinc doped ferrites

#### 4.3.1. Zinc ferrites

Gas sensing of Zinc ferrites have been studied and found to have various efficiencies or lack of on the following gases, LPG,<sup>48,85,118,168</sup> Acetone,<sup>85</sup> ammonia ( $NH_3$ ),<sup>176</sup> methanol,<sup>176</sup> ethanol ( $C_2H_5OH$ ),<sup>85,118,176–180</sup> hydrogen ( $H_2$ ),<sup>13,97,115,176,180</sup>  $NO_x$ ,<sup>180</sup>  $SO_x$ ,<sup>177</sup>  $H_2S$ ,<sup>177,178</sup> Carbon monoxide (CO),<sup>13,115,118,181</sup> Methane ( $CH_4$ ),<sup>115,118</sup> Nitrogen dioxide ( $N_2O$ )<sup>118</sup> and acetone.<sup>176</sup>

Darsane et al.<sup>177</sup> prepared  $ZnFe_2O_4$  nanoparticles by the molten salt route and examined its sensing properties toward  $NO_x$ ,  $SO_x$  and  $H_2S$ . From XRD analysis single Phase formation of  $ZnFe_2O_4$  of crystallite

size ranging from 15–20 nm were observed. The sensors were calcined at 700 °C. The particle size calculated using Scherer formula showed particle size of 16 nm. It was observed that sensor exhibited highly selective sensitivity toward 200 ppm of  $H_2S$  at working temperature of 200 °C. The response toward  $H_2S$  was found to be 330 while for  $H_2$ ,  $NO_2$ , acetone and ethanol it was less than 60. Rezlescu et al.<sup>65</sup> prepared  $ZnFe_2O_4$  through sol-gel self-combustion method and studied its ethanol, acetone and LPG sensing properties. Ferrites were heat treated at 1000 °C to impact ceramic properties. Ferrite was characterized with smaller grain size of 100 nm, porosity of 48.4% and large active surface of 22.2 m<sup>2</sup>/g toward test gases. The maximum sensitivity of the tested gases at a concentration of 150 ppm each were obtained at 350 °C. Maximum sensitivity was found to be 90% with response time of about 3 minutes and recovery time of 2 minutes. Zhu et al.<sup>180</sup> prepared  $ZnFe_2O_4$  nanorods through micro-emulsions based synthesis and studied their application as ethanol sensor at a room temperature. TEM images showed that ferrite consisted nanocrystals ranging from 5 nm to 10 nm which arranged in line. Large number of nanoholes enhanced specific surface area which resulted to increase in ethanol response. It was found that response increased from 14–2380 as concentration increased from 50 ppm to a maximum of 500 ppm. Jiao et al.<sup>118</sup> prepared  $ZnFe_2O_4$  films by ultrasonic spray pyrolysis on alumina substrates. Sensing properties of the substrates were examined toward 500 ppm of CO,  $CH_4$ ,  $C_2H_5OH$  and LPG. It was found from SEM that  $ZnFe_2O_4$  film had a very good adherence to the substrate having spherical particles with mean size of about 200 nm. The sensitivity toward CO was found to be 10 while for  $CH_4$ ,  $C_2H_5OH$  and LPG were 2.0, 1.6 and 1.4 respectively.

Tyagi et al.<sup>179</sup> prepared  $ZnFe_2O_4$  through auto-combustion method and examined its sensing properties toward ethanol. From FESEM micrographs the particles of the synthesized ferrites were found to have spherical shaped morphology with the particle ranging from 10–15 nm. On heat treatment the particle size increased to the range of 35–40 nm. Sensitivity was observed to be dependent of both working temperature and concentration. As temperature increased, sensitivity increased as concentration increased from 200–800 ppm. Maximum sensitivity for “as synthesized” material appeared at 250 °C while for heat treated at 300 °C. Calcined ferrite showed a faster response of 65 s and a recovery time of 75 s while for “as synthesized” had a response of 70 s and recovery

time of 90 s. Singh et al.<sup>48</sup> examined sensing properties of ZnFe<sub>2</sub>O<sub>4</sub> nanorods toward LPG. Samples were synthesized through sol-gel auto-combustion technique. The diameters of the rods were found to be in the range of 30 nm to 40 nm, length ranging from 100–120 nm whereas specific surface area was found to be 86.47 m<sup>2</sup>/g. The size of crystallites was calculated using Debye Scherrer formula was found to be 10 nm. The maximum sensitivity and percentage sensor response toward 2000 ppm of LPG were found to be 2.4 and 140% respectively. The response time as well as the recovery time were found at approximately 60 s and 300 s.

#### 4.3.2. Zinc doped ferrites

Zinc ions have been substituted with magnesium<sup>115,181–185</sup> in a bid to improve one of the sensing parameters mentioned in § 2. Maity et al.<sup>184</sup> prepared Mg<sub>0.5</sub>Zn<sub>0.5</sub>Fe<sub>2</sub>O<sub>4</sub> through self-combustion route and examined its sensitivity toward H<sub>2</sub>, CH<sub>4</sub> and CO. The synthesized nanocrystalline powder was made in pellet and calcined at 600 °C for 2 h to form circular sensing element. All test the test gases were examined at a concentration ranging from 500–1660 ppm at working temperature ranging from 250 °C–380 °C. It was found that response was dependent of both working temperature and concentration up-to a particular point where it start to reduce. Jain et al.<sup>186</sup> studied LPG sensing properties of Zn<sub>1-x</sub>Cu<sub>x</sub>Fe<sub>2</sub>O<sub>4</sub> (x = 0.0, 0.25, 0.5 and 0.75) prepared through sol-gel auto-combustion method. The samples were sintered at 650 °C for 4.5 h to enhance sensing characteristics. XRD showed that zinc copper ferrite exhibited single phase inverse spinel structure. With increased concentration of copper, the size of crystallite was observed to increase from 28 nm to 47 nm. Morphological analysis from SEM showed ferrite exhibited a structure which was porous of particles throughout the sample. LPG response linearly depended on operating temperature concentration and composition. Maximum sensitivity of 55.35% for 0.6 vol% of LPG at 250 °C for Zn<sub>0.5</sub>Cu<sub>0.75</sub>Fe<sub>2</sub>O<sub>4</sub> was observed. Both response time and recovery time were observed at 6.25 and 3.5 min respectively.

### 4.4. Copper ferrites and copper doped ferrites

#### 4.4.1. Copper ferrites

Studies have reported various sensing efficiencies for copper ferrites in presence of the following gases; LPG,<sup>85,187–189</sup> ammonia (NH<sub>3</sub>),<sup>26</sup> ethanol (C<sub>2</sub>H<sub>5</sub>OH),<sup>26,85,189</sup> acetone (CH<sub>3</sub>COCH<sub>3</sub>),<sup>26,85</sup> carbon monoxide (CO),<sup>189</sup> carbon dioxide (CO<sub>2</sub>),<sup>189–191</sup>

hydrogen (H<sub>2</sub>),<sup>26,189,192</sup> hydrogen sulfide,<sup>193</sup> gasoline<sup>189</sup> and acetylene.<sup>189</sup>

Rezlescu et al.<sup>65</sup> prepared CuFe<sub>2</sub>O<sub>4</sub> through sol-gel auto-combustion technique and examined its ethanol, acetone and LPG sensing properties. It was observed that the ferrite exhibited large faceted crystallite of 700 nm and have a tendency toward agglomeration as a result of the smaller size of the ferrite particle. It was also characterized with porosity of 32.8% and surface specific area of 2.4 m<sup>2</sup>/g. The maximum sensitivity of each test gas was observed at a gas concentration of 150 ppm and operating temperature of 350 °C. Maximum sensitivity of 90% was attained at response of 3 minutes and recovery time of 4 minutes.<sup>194</sup> fabricated CuFe<sub>2</sub>O<sub>4</sub> porous hierarchical nanostructure through sol-gel coating method and examined its sensitivity toward LPG. SEM micrographs showed that CuFe<sub>2</sub>O<sub>4</sub> film had porous surface morphology with pore size ≈150–700 nm thereby enhancing sensitivity. The size of the particle was found to be 12 nm and average of 13 nm both determined using Debye Scherrer equation. It was observed that maximum sensitivity was 1.96 for 500 ppm of LPG. Both response time and recovery time were found at ≈0 s and ≈400 s respectively. Haija et al.<sup>193</sup> studied H<sub>2</sub>S sensing properties of CuFe<sub>2</sub>O<sub>4</sub> nanoparticles prepared through sol-gel self-combustion. They were annealed at 500 °C and 750 °C. The crystallites increased from 27 nm as prepared to 32 nm for both annealed samples. Maximum sensitivity of the sensors toward 25 ppm of H<sub>2</sub>S was observed at 80 °C. The response time was found to be 51.5 ± 3.4 s for both as synthesized and calcined at 750 °C samples and almost twice for samples calcined at 500 °C.

#### 4.4.2. Copper doped ferrites

Copper substituted with Cerium,<sup>175,195</sup> with manganese,<sup>83,196</sup> with Lithium,<sup>197</sup> with Zinc<sup>186</sup> and platinum.<sup>198,199</sup> studied magnetic dielectric and LPG sensing properties of Mn<sub>0.4</sub>Cu<sub>0.6</sub>Fe<sub>2</sub>O<sub>4</sub> prepared through self-combustion method. The samples were calcined at 600 °C and 900 °C for 5 hours. The size crystallite calculated from XRD was observed in the range of ≈–45 nm from the TEM spherical particle in the range of 40–60 nm was observed. It was observed that sensor response increased linearly with concentration of LPG and operating temperature. Maximum response was attained at concentration of 1000 ppm at 300 °C.



## 4.5. Cadmium ferrites and cadmium doped ferrites

### 4.5.1. Cadmium ferrites

Rezlescu et al.<sup>25</sup> studied acetone, C<sub>2</sub>H<sub>5</sub>OH and LPG sensitivity by CdFe<sub>2</sub>O<sub>4</sub> prepared through sol-gel auto-combustion. The sensor in pellet form was sintered at 100 °C for 30 min to facilitate solid state. From XRD and SEM analysis average grain size of 30 nm, porosity of 45.5% and surface specific area of 6.0 were found. Maximum sensitivity for the test gases appeared at 350 °C and at concentration of 150 ppm. It was also found that CdFe<sub>2</sub>O<sub>4</sub> exhibited highest sensitivity toward alcohol and less sensitive toward LPG and Acetone.

Chen et al.<sup>136</sup> examined LPG sensing properties of CdFe<sub>2</sub>O<sub>4</sub> synthesized by co-precipitate method. XRD result showed that the samples exhibited single phase spinel-type structure with crystal size of 33 nm. TEM images portrayed the samples particles had spherical shape with mean diameter within 50 nm and surface area of 80.1 m<sup>2</sup>/g. Highest sensitivity toward 2000 ppm of LPG appeared at 250 °C. Rezlescu et al.<sup>25</sup> studied LPG, C<sub>2</sub>H<sub>5</sub>OH and acetone sensing characteristic of CdFe<sub>2</sub>O<sub>4</sub> prepared through sol-gel auto-combustion technique. The pellets sensors were sintered at 1000 °C for 30 min to facilitate solid state of ferrites. XRD and SEM analysis showed the ferrites had a porosity of 45.5%, the size of the crystallite 300 nm and specific areas of 6.0 m<sup>2</sup>/g were observed. At 150 ppm of test gases and at operating temperature of 350 °C, it was observed that CdFe<sub>2</sub>O<sub>4</sub> was more sensitive to alcohol and as compared to LPG and acetone.

Tianshu et al.<sup>199</sup> studied ethanol sensing properties of CdFe<sub>2</sub>O<sub>4</sub> prepared through chemical co-precipitation technique. Samples were sintered at 600 °C and 800 °C so as to enhance sensing properties. XRD analysis confirmed single phase of CdFe<sub>2</sub>O<sub>4</sub> and the sizes of crystallite were estimated to be 15 nm. Spheroidal particles of size 30 nm were observed from SEM micrographs. Maximum sensitivity of 90% toward 200 ppm ethanol vapor was observed at 380 °C with both response time and recovery time recorded at 15 s and 35 s respectively. Gadkari et al.<sup>200</sup> examined sensing properties of CdFe<sub>2</sub>O<sub>4</sub> synthesized by oxalate co-precipitation technique toward LPG, Cl<sub>2</sub>, and ethanol. XRD showed the formation of single phase cubic spinel structure. The size of Crystallites calculated using Scherrer formula was found to be 30 nm. Maximum sensitivities of 85%, 35% and 30% were found toward ethanol, LPG and Cl<sub>2</sub> respectively were found. Both response time and recovery time toward LPG were 200 s and 250 s respectively, 200 s and 350 s toward Cl<sub>2</sub> while 250 s and 300 s toward ethanol respectively.

### 4.5.2. Cadmium doped ferrites

Kotresh et al.<sup>201</sup> studied LPG sensing characteristic of PANI-CdFe<sub>2</sub>O<sub>4</sub> prepared by chemical polymerization. The obtained powder was calcined at 300 °C. From XRD analysis, the size of the crystallites was found to be 24 nm for CdFe<sub>2</sub>O<sub>4</sub> and 30 nm for the PANI-CdFe<sub>2</sub>O<sub>4</sub>. FESEM images showed homogenous porous morphology with high surface area. Maximum response of 50.83% toward 100 ppm OF LPG at a room temperature was observed. Both response time and recovery time were found at 50 s and 100 s respectively were observed while stability was found to exceed a period of 1 month with a small change of 4%. Chethan et al.<sup>202</sup> studied humidity sensing properties of Cd<sub>1-x</sub>Ni<sub>x</sub>Fe<sub>2</sub>O<sub>4</sub> (x = 0.0 and 0.5) synthesized through sol-gel auto-combustion technique. The powders were calcined at 400 °C. XRD confirmed cubic spinel structure thus showing its polycrystalline in nature. The average size of the grain of both pure and substituted was found to be 0.6 μm and 0.3 μm respectively. At room temperature maximum response of 99% and 50% were observed for substituted and pure CdFe<sub>2</sub>O<sub>4</sub> respectively when measured in the range of 25–95% RH. Response time as well recovery time were found to be 30 s and 45 s for nickel substituted and 123 s and 154 s for CdFe<sub>2</sub>O<sub>4</sub>.

## 4.6. Magnesium ferrites and magnesium doped ferrites

### 4.6.1. Magnesium ferrites

Patil et al.<sup>114</sup> examined LPG, NH<sub>3</sub>, ethanol and acetone sensing properties of MgFe<sub>2</sub>O<sub>4</sub> prepared through sol-gel auto-combustion. Ferrite was sintered at 1173 K. From XRD it was observed that the size of the particle increased from 30 to 38 nm with sintering temperature. The response of about 71% to 200 ppm of LPG was found at 698 K. Hankare et al.<sup>123</sup> examined gas sensing properties of MgFe<sub>2</sub>O<sub>4</sub> synthesized through co-precipitation route. The ferrite was sintered at 900 °C for 4 h to enhance sensing properties. From SEM the size of the particle tabulated using Cottrell's method was about 1 μm. This suggested formation of grain through aggregation of small crystallites of 40 nm. It was found that sensitivities of ferrite toward petrol, ethanol, methanol, LPG and ammonia greatly depended on operating temperature as well as concentration. Maximum sensitivity of 3.0 at 250 °C of 5 ppm petrol was recorded. Liu et al.<sup>203</sup> examined gas sensing of MgFe<sub>2</sub>O<sub>4</sub> synthesized by solid state reaction. The samples were annealed at 700 °C. The resulting MgFe<sub>2</sub>O<sub>4</sub> consisted particles of size ranging

from 15–30 nm. The gas sensing responses toward CH<sub>4</sub>, LPG, ethanol (C<sub>2</sub>H<sub>5</sub>OH) were found to increase linearly with temperature up to a certain temperature where it began to decrease for ethanol. Maximum response was found at 355 °C while for H<sub>2</sub>S, was found at 160 °C. It was also observed that there was a linear relationship between the sensitivity and gas sensing. Godbole et al.<sup>204</sup> Studied alcohol sensing properties of MgFe<sub>2</sub>O<sub>4</sub> prepared using auto-combustion method. From XRD it was found that the samples exhibited spinel phase. The particles were observed to be spherical in shape with the size averaging to 15–20 nm and pore size of ≈ μm. Maximum sensitivity of 73% toward 5 ppm C<sub>2</sub>H<sub>5</sub>OH was found at 275 °C while sensitivity of 50% was observed for 5 ppm CH<sub>3</sub>OH.

#### 4.6.2. Magnesium doped ferrites

Bharti et al.<sup>182</sup> prepared Mg<sub>1-x</sub>Zn<sub>x</sub>Fe<sub>2</sub>O<sub>4</sub> (x ranges from 0.1–1.0) through wet chemical preparation route and examined its sensing characteristic toward H<sub>2</sub> and CO. The powders were calcined at the range of 300–900 °C for 2 h in air. From XRD analysis the size of the crystallite size was found to be approximately 11 nm. Sensitivity of 44% of 1660 ppm of CO was achieved at operating temperature of 320 °C. On the same concentration, sensitivity of 65% was observed for H<sub>2</sub> at the operating temperature of 380 °C. Patil et al.<sup>205</sup> examined acetone sensing properties of MgFe<sub>2-x</sub>Ce<sub>x</sub>O<sub>4</sub> (x ranges from 0.04 to 0.12) prepared through sol gel self-auto-combustion method. The samples were sintered at 973 K and 1173 K. It was observed that with Ce increase the crystal size decreased gradually SEM micrographs showed porous microstructure which enhanced sensor response. As Ce doping increased from x = 0.04 to x = 0.12 the size of the grain was observed to decrease from 0.24, 0.13 to 0.07 μ m. XRD analysis showed that the size of crystallite to be in the range of 28–34 nm. It was found that sensor response linearly increased with temperature and saturated at optimum temperature. Maximum response of 94% at 598 K was observed for x = 0.12. Thick film sensor sintered at 973 K. The corresponding response time and recovery time were recorded at 20 s and 65 s accordingly.

Darshane et al.<sup>206</sup> examined sensing performance of Pd doped MgFe<sub>2</sub>O<sub>4</sub> synthesized through molten salt route. The samples were annealed at 700 °C to enhance ceramic properties. XRD showed single-phase formation of both pure and doped MgFe<sub>2</sub>O<sub>4</sub> having the size of crystallite ranging from 15–20 nm. It was observed that Pd improved selectivity to LPG

and reduced toward H<sub>2</sub>, C<sub>2</sub>H<sub>5</sub>OH, NO<sub>x</sub>, SO<sub>x</sub>, H<sub>2</sub>S as well as acetone. Maximum response of ≈0 for pure MgFe<sub>2</sub>O<sub>4</sub>, ≈70 for 1% doped and ≈430 for 3% doped were recorded toward 200 ppm of LPG at 200 °C. Pure MgFe<sub>2</sub>O<sub>4</sub> showed response and recovery times at 5 s and 5 min respectively while for 1% doped and 3% doped at response of 3 s and 2 s respectively and both having a recovery time of 2 min. Kotnala et al.<sup>207</sup> studied humidity sensing properties of Mg<sub>1-x</sub>Li<sub>x</sub>Fe<sub>x</sub>O<sub>4</sub> (0.0 ≤ x ≤ 0.6) synthesized through solid state reaction method. The pellet sensors were annealed at 300 °C to enhance ceramic properties. XRD analysis showed the samples exhibited spinel structure. As lithium ions increased it was found that the size of the grain reduced from 200 nm to 110 nm. Sensitivity factor was found to increase in the range of 165 for pure ferrite to 2080 for lithium substitution in the range 10–80% RH. The shortest time measured was 180 s for the x = 0.4 sample. The porosity decreased as Li content increased from 9.7% for x = 0.2 to 2.6% for 0.4. On the other hand fastest response time was observed at 180 s for x = 0.4 while recovery time was 435 s for x = 0.6.

#### 4.7. Manganese ferrites and manganese doped ferrites

##### 4.7.1. Manganese ferrites

Rathore et al.<sup>208</sup> studied SO<sub>2</sub> and NO<sub>2</sub> sensing characteristic of MnFe<sub>2</sub>O<sub>4</sub> synthesized by chemical co-precipitate method. XRD showed that the ferrite formed a single phase cubic structure. The size of the crystallite was determined using Scherrer formula and was found to be 10.7 nm. It was observed that MnFe<sub>2</sub>O<sub>4</sub> nanoparticles were more sensible for NO<sub>2</sub> at 93.6% as compared to SO<sub>2</sub> at 80.6%. Recovery and response time for both gases were 1 s and 5 min respectively. Vignesh et al.<sup>209</sup> studied NH<sub>3</sub> sensing properties of MnFe<sub>2</sub>O<sub>4</sub> prepared through solution assisted combustion method. XRD analysis revealed that the sample exhibited spinel cubic structure. The average size of the particle was found to be in the range of 30–35 nm. Maximum sensitivity of 83.5% toward 10 ppm of NH<sub>3</sub> was observed at 300 K.

##### 4.7.2. Manganese doped ferrites

Satyanarayana et al.<sup>79</sup> synthesized Ni<sub>1-x</sub>Co<sub>x</sub>Mn<sub>x</sub>Fe<sub>2-x</sub>O<sub>4</sub> by hydrazine method and examined its sensing behavior toward LPG, C<sub>2</sub>H<sub>5</sub>OH, Co and CH<sub>4</sub>. The powder was calcined at 500 °C to complete crystallization in to the cubic spinel phase. From XRD analysis the size of the crystallite was calculated using Debye Scherrer formula and was found to be in the range of 10–15 nm. Specific

surface area on the other hand was found to be  $60 \text{ m}^2/\text{g}$ . It was observed that upon incorporation of 1 wt.% Pd, sensitivity increased, and response time reduced and the operating temperature of the sensor also lowered. Maximum sensitivity of  $\approx 60\%$  was observed for 1000 ppm of LPG at  $180^\circ\text{C}$ . The response time was found to be less than 1 min. Koseoglu et al.<sup>210</sup> synthesized  $\text{Mn}_{0.2}\text{Ni}_{0.8}\text{Fe}_2\text{O}_4$  nanoparticles by PEG assisted hydrothermal route and studied humidity sensing properties. From XRD analysis, the size of the crystallite was calculated using Debye Scherrer formula was found to be 27 nm. SEM micrographs showed that nanoparticles exhibited large grain structure having irregular morphology with soft agglomeration. Sensitivity was observed to increase with concentration from 1000 ppm to 8000 ppm where it saturated. Highest sensitivity of 0.99 was found at  $250^\circ\text{C}$  for 8000 ppm of humidity. Response time as well as recovery time were found to be 450 s and 90 s respectively.

#### 4.8. Lithium and lithium doped ferrites

Rezlescu et al.<sup>25</sup> examined gas sensing properties of  $\text{Li}_{0.5}\text{Sm}_x\text{Fe}_{2.5}\text{O}_4$  for ( $x = 0, 0.05, 0.1$  and  $0.2$ ) synthesized using sol-gel self-combustion method. The disk sensor was sintered at  $850^\circ\text{C}$  for 2 hours from SEM images samples exhibited high porosity as well as small particle size, under  $0.2 \mu\text{m}$  with increasing Sm content, the size of particle the decreased from  $0.2$  to  $(0.1\text{--}0.15) \mu\text{m}$  and porosity increased from 33.2% to about 44%. It was further found that sensitivity depend on, the working temperature, porosity, concentration of the gas as well as the gas type. For instance 200 ppm of ethanol or methanol vapor, maximum sensitivity of 80–87% and response of about 3 min was observed at working temperature range of  $340\text{--}355^\circ\text{C}$ . The recovery time was found to be longer at about (5–6 min). Manikandan et al.<sup>154</sup> synthesized ( $\text{Li-CuFe}_2\text{O}_4$ ) using co-precipitation method and fabrication into thin film for gas sensing. The prepared thin film was calcined at  $900^\circ\text{C}$  for 4 hours and then used as sensor toward LPG. The XRD revealed cubic structure with the size of crystallite and lattice constant of thin film found at  $\approx 7 \text{ nm}$  and 8.303 angstroms. TEM images showed irregular particle sizes in the range of 7–17 nm. It 2 as found that sensor response increased with LPG concentration from (0.5 to 4 vol %). The maximum sensitivity of 83.82% was observed for 4 Vol to a room temperature. The observed response time and recovery time were 2.7 and 19.36 minutes respectively.

## 5. Methods of synthesis of gas sensing spinel ferrites

Synthesis techniques play key role in controlling the size and surface area as well of ferrite material. The preparation of ferrite nanoparticles for gas sensing has been studied using different methods which *inter alia* includes; sol-gel self-combustion, co-precipitation, wet chemical method, solid state reaction, ball milling, hydrothermal and molten salt as summarized in figure 4.

### 5.1. Sol-gel auto-combustion method

It consists of exothermic and self-sustaining thermally induced reaction of xerogel (redox reaction of xerogel), see Figure 5.<sup>47</sup>

For ferrites synthesis, metal nitrates are preferred as oxidizer and citric acid monohydrates as reductant. Ferrites nanoparticles are formed as a result of emission of large volume of gas which is accompanied by loss of large mass during the xerogel combustion process. This technique has widely been used to synthesis ferrites for sensing detection. Rezlescu et al.<sup>65</sup> synthesized  $\text{CuFe}_2\text{O}_4$ ,  $\text{CdFe}_2\text{O}_4$  and  $\text{ZnFe}_2\text{O}_4$  via sol-gel and examined their LPG, acetone and ethanol sensing characteristics. In the synthesis process, appropriate metal nitrates were weighed in the required amount and thereafter were dissolved in distilled water. Alcohol polyvinyl was added to make a colloidal solution. Ph of 8 was maintained by adding  $\text{NH}_4\text{OH}$  solution and this resulted to the sol of metal hydroxide and ammonium nitrates. The sol was therefore heated at  $120^\circ\text{C}$  for 12 h and the gel obtained was ignited. The combustion converted gel into a loose powder containing very fine crystallite. In order to eliminate organic compounds, the powders were heated at  $500^\circ\text{C}$ .

Other studies which have employed the method to synthesis ferrite for gas sensing includes; Jain et al.<sup>186</sup> Synthesized  $\text{Zn}_{1-x}\text{Cu}_x\text{Fe}_2\text{O}_4$  for LPG sensing, Singh et al.<sup>165</sup> synthesized  $\text{ZnFe}_2\text{O}_4$  for ethanol sensing, Patil et al.<sup>119</sup> synthesized  $\text{NiFe}_2\text{O}_4$  for LPG, acetone and alcohol sensing etc. Advantages of using this method of synthesis includes; better chemical homogeneity, purity of the product as well as the crystallinity, particle size being fines, simple step followed, low external energy consumption, easy to control stoichiometry and simple equipment preparation process. The mentioned advantages as an example are evidenced in the study of  $\text{ZnFe}_2\text{O}_4$ ,  $\text{CuFe}_2\text{O}_4$  and  $\text{CdFe}_2\text{O}_4$  as LPG, acetone and ethanol sensors.<sup>81</sup> Small particle size, homogeneity in grain distribution, purity, crystallinity as well as tendency toward agglomeration due to the small size of the ferrites were obtained. Properties of

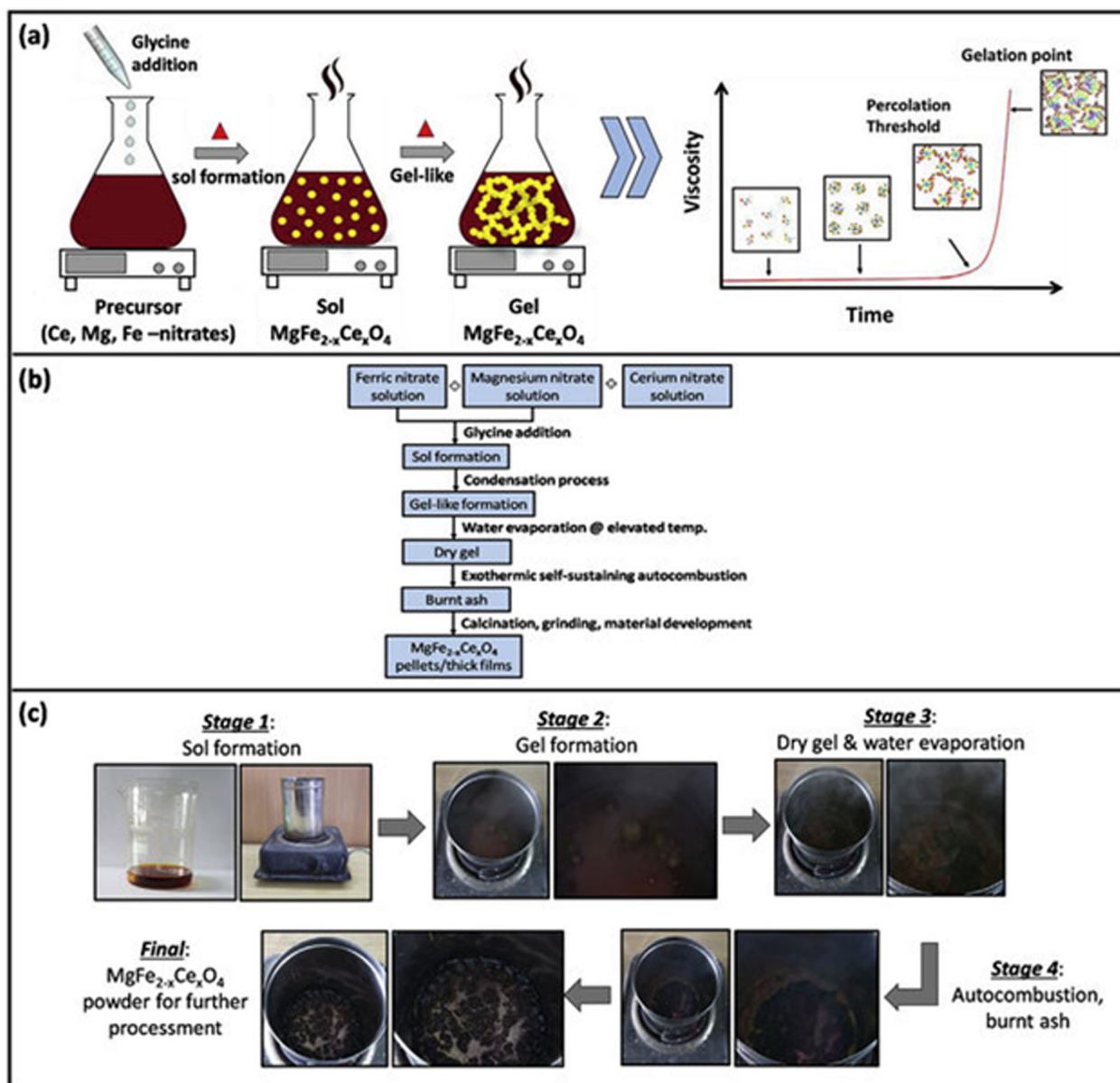


**Figure 5.** Schematic of complete sol-gel synthesis route, here showing synthesis of Cerium doped  $MgFe_2O_4$  (a) illustration of sol-gel combustion reaction alongside viscosity graph (b) experimental flow chart (c) photographs of transitional step from reaction to final product, obtained from Patil et al 11.

ferrites prepared using sol-gel method are affected by; fuel agent, reductant to metal salt ratio, combustion process chemical additives and heating mechanism. Some of them are discussed below.

### 5.1.1. Reductant to metal salt ratio

The ratio of reductant to metal nitrates reaction is very important since it allow control of flame time which affects the formation growth of the phase as well as on the particle agglomeration state.<sup>211</sup> Whenever the excess complexant is used the rate of reaction as well as temperature are reduced hence oxygen in extreme need to be supplied. Furthermore,

with large complexant amount, large gases volume is produced and hence reduces chances of particles to contact, growth and as well as to sinter to each other. This produces high specific area powders.<sup>212</sup> On the other hand for the smaller amount of reductant, the heat produced is not sufficient due to lack of complexant in the process. The reaction rate and temperature are thus reduced and as a result there is particle size decrease and increase in specific surface area.<sup>213</sup> Kapse<sup>1</sup> in the synthesis of  $NiFe_2O_4$ ,  $MgFe_2O_4$  and  $ZnFe_2O_4$  for gas sensing applications, mixed appropriate metal nitrates with citric acid monohydrates which acts as a fuel agent in the proportion of 1:3

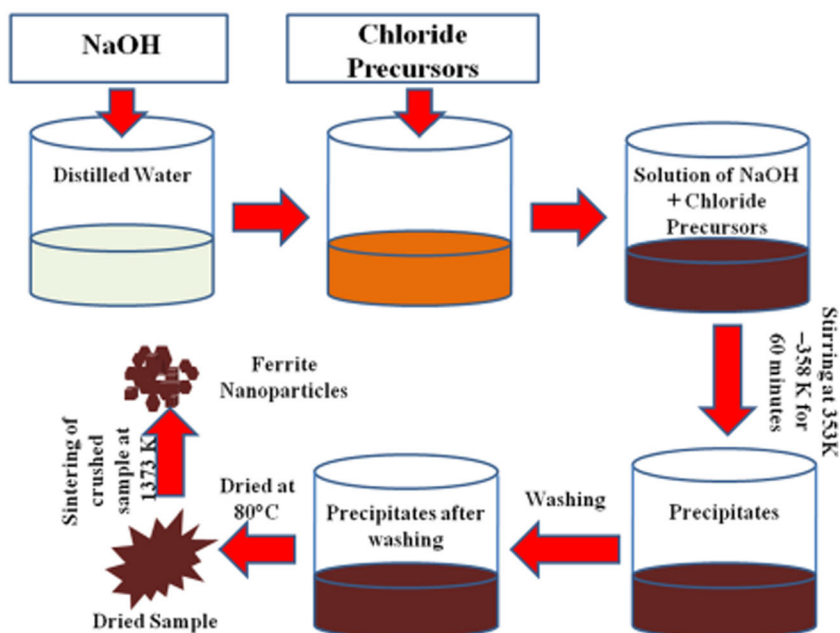


**Figure 6.** Schematic diagram of co-precipitation method to synthesize  $\text{Mn}_{0.5}\text{Zn}_{0.5}\text{La}_x\text{Fe}_{2-x}\text{O}_4$  ( $x = 0, 0.025, 0.050, 0.075$  and  $0.1$ ) ferrites. Figure obtained from Thakur et al.<sup>216</sup>

respectively. Gedam et al.<sup>169</sup> in the preparation of  $\text{Co}_{0.8}\text{Ni}_{0.2}\text{Fe}_2\text{O}_4$  ammonia gas sensor, appropriate stoichiometric amount of metal nitrates were mixed with citric acid monohydrates. Godbole et al.<sup>204</sup> in the synthesis of  $\text{MgFe}_2\text{O}_4$  nanoparticles for alcohol sensing appropriate metal nitrates were mixed with glycine in the ratio of 1:1. Patil et al.<sup>114</sup> in the synthesis of  $\text{MgFe}_2\text{O}_4$  for LPG sensing appropriate metal nitrates were mixed with glycine in the ratio of 3:5.

### 5.1.2. Combustion process chemical additives (CPCA)

For the purpose of improving combustion of gel many CPCA are used. Some includes;  $\text{NH}_4\text{NO}_3$ ,<sup>47</sup>  $\text{NH}_4\text{OH}$ <sup>1</sup> and  $\text{C}_2\text{H}_4$  ( $\text{NH}_2$ ).<sup>214</sup> When citric acid is used as reductant,  $\text{NH}_4\text{OH}$  is always added to aid in increasing metal cations chelating with citrates.<sup>215</sup>

### 5.2. Co-precipitation method

This is a low temperature synthesis technique for precipitating nano-particles from aqueous solution of metal salt in basic condition.<sup>47</sup> its procedure is schematized graphically in Figure 6.<sup>216</sup>

At lower temperature about  $100^\circ\text{C}$ , the size of the particle obtained are smaller than 100 nm. Precursors, molarity, temperature, pH as well as time affects phase purity, aspect ratio, stoichiometry inversion and point defects of the spinel ferrites nanoparticles concentration.<sup>217</sup> The characteristics of the spinel ferrites nanoparticles synthesized are reproducible only when the

co-precipitation conditions are fixed. Ferrites with additional (oxy)-hydrate, amorphous impurity phases as well as low crystallinity are produced as a result of low synthesis temperature.<sup>218</sup> To increase crystallinity as well as phase purity the obtained powder are annealed at high temperature (above  $500^\circ\text{C}$ ). Abdel et al.<sup>219</sup> synthesized  $\text{NiFe}_2\text{O}_4$  through co-precipitate method for gas sensing applications. From the chemical reaction of solution of pure sodium hydroxide with solution of pure chloride of nickel and iron. The co-precipitated powder at pH of 12.5 and at a temperature of  $85^\circ\text{C}$   $\text{NiFe}_2\text{O}_4$  is formed. The crystallite of co-precipitated powder without any annealing was found to be 74.93 nm while for annealed powder at  $1000^\circ\text{C}$  for 6 h was 225.45 nm. The increase of the crystallinity size led to the reduction in the sensitivity. Gadkari et al.<sup>200</sup> prepared ethanol sensor based on nanocrystalline  $\text{CdFe}_2\text{O}_4$  through co-precipitate method. The preparation was done using AR grade cadmium and ferrous sulfate. The precipitate was pre-sintered for 6 h in air and finally was calcined at  $1050^\circ\text{C}$  for 5 h in air. Upon sintering the size of crystallites were found to be 30.4 nm which is suitable for gas sensing application.

Other studies which has synthesized ferrites sensors through this methods includes; Tianshu et al.<sup>199</sup> synthesized ethanol sensor based on  $\text{CdFe}_2\text{O}_4$ , Rezlescu et al.<sup>25</sup> prepared  $\text{NiFe}_2\text{O}_4$  through co-precipitate method for gas sensing applications. Generally once the co-precipitation conditions are adjusted samples obtained are pure, increased crystallite size and hence reduced resistivity which increases sensitivity toward test gas.

### 5.3. Solid-state reaction method

This method of synthesizing ferrite is done by mixing raw materials which takes place with wet and dry process.<sup>54</sup> An aqueous suspension, vibration drum or agitator is used in wet mixing method. This technique produces excellent ferrite for gas sensing but on the other hand it requires energy for dewatering as well as drying. Dry mixing is done either by grinding and mixing in a drum or ballmill. Kotnala et al.<sup>207</sup> synthesized lithium substituted  $\text{MgFe}_2\text{O}_4$  by solid state reaction for application in humidity sensing. Analytical grade reagent  $\text{MgSO}_4$ ,  $\text{LiNO}_3$ ,  $\text{Fe}(\text{NO}_3)_3 \cdot 9\text{H}_2\text{O}$ ,  $\text{NaOH}$  and  $\text{NaCl}$  were used in the appropriate proportions. Sodium hydroxide was added so as to change metal nitrates and sulfates into hydroxides while on the other hand  $\text{NaCl}$  was added for the purposes of restricting the grains growth so as to keep them in small size as possible. The mixture was then grounded in an agate motor with a pastel for about 1 h. An exothermic reaction first resulted to an aqueous mixture which was dark red which thereafter slowly transformed into a paste which was brown in color. Then Paste was calcined at  $750^\circ\text{C}$  for 3 h in a furnace. Finally the calcined mixture was washed with deionized water and thereafter dried at temperature of  $120^\circ\text{C}$  overnight. The obtained ferrite provides suitable characteristic for gas sensing for example high porosity ranging from 2.6–8.9%, grain distribution of 250 nm to  $1.6\ \mu\text{m}$  as well as surface structure showed that grain through the grain necks were well connected.

In another study, Scherrer et al.<sup>67</sup> synthesized  $\text{NiFe}_2\text{O}_4$  nanopowder doped with noble metal for the application as  $\text{H}_2\text{S}$  sensor. In the synthesis process analytical grade  $\text{Ni}(\text{Ac})_2$ ,  $\text{Fe}(\text{NO}_3)_3$  and  $\text{NaOH}$  were mixed in equimolar proportions and grounded together in an agate motor for about 30 min. Afterwards  $\text{NaCl}$  was added so as to avoid agglomeration. The resulting mixture was sintered at  $700^\circ\text{C}$  for 1 h. afterwards, the powder was washed with deionized water for severally and finally dried at  $100^\circ\text{C}$  for 2 h. Generally, solid-state reaction is widely used method in the synthesis of ferrites for gas sensing application due to; simple step followed, purity and crystallinity of the samples and high porosity as seen from above examples.

### 5.4. Wet chemical method

Wet chemical technique has been widely reported in synthesizing ferrites nanoparticles for gas sensing applications. Karmakar et al.<sup>183</sup> synthesized  $\text{Mg}_{0.5}\text{Zn}_{0.5}\text{Fe}_2\text{O}_4$  for acetone and ethanol sensing.

Ferrite was synthesized from the nitrates precursor salt of zinc, magnesium as well as iron using ethylene glycol and citric acid. Precursor salt was first dissolved in water and afterwards, appropriate amount of ethylene glycol as well as citric acid were added to the mixture. The complex precursor was stirred for 4 h at  $80^\circ\text{C}$  and finally heat treated at a temperature of  $120^\circ\text{C}$  until self-combustion occurred. At the end of the self-combustion  $\text{Mg}_{0.5}\text{Zn}_{0.5}\text{Fe}_2\text{O}_4$  powder was obtained. Powder was sintered at  $750^\circ\text{C}$  to produce nanoparticles which were crystalline in nature. XRD revealed that the ferrite prepared had no impurity phases, high crystallinity, small crystallites of size  $\approx 23\ \text{nm}$  and particle size of  $\approx 58\ \text{nm}$ . Leroux et al.<sup>167</sup> synthesized cobalt ferrites for  $\text{NH}_3$  sensing by wet chemical route. The ferrite produced exhibited high crystallinity, homogenous in composition, size and well dispersed. From the above examples, wet chemical method produces spinel ferrites with high crystallinity, purity, homogeneity and porosity which are essential properties to gas sensing.

### 5.5. Molten-salt method

Darshane et al.<sup>177</sup> used the method to synthesize  $\text{ZnFe}_2\text{O}_4$  for gas sensing applications. In the process,  $\text{ZnSO}_4$ ,  $\text{Fe}(\text{NO}_3)_3$ ,  $\text{NaOH}$  as well as  $\text{NaCl}$  were mixed in the appropriate proportion and were together grounded for 90 min. During the mixing, heat was released as the reaction was taking place. At first, the mixture turned mushy afterward it gradually changed from colorless to light red and for a few minutes it turned to brown. Afterwards, the mixture was heat treated at  $700^\circ\text{C}$  for 90 min and thereafter cooled to a room temperature. Finally the sample was washed severally with distilled water and dried at a temperature of  $120^\circ\text{C}$  for 4 h. Nanocrystallite single phase of  $\approx 16\ \text{nm}$  spinel  $\text{ZnFe}_2\text{O}_4$  was found at a relatively low processing temperature and for a short duration hence advantage of the method.

## 6. Conclusion

According to available literature and reviews as well as publications on ferrite gas sensors show that sol-gel auto-combustion method is preferred to synthesize a wide variety of ferrite gas sensing material. The sensor properties which include; working temperature, selectivity, sensitivity response time as well as recovery time depends on preparation techniques, calcination temperature, gas type as well as the concentration of the gas. Various gases show different gas sensing behavior.

MgFe<sub>2</sub>O<sub>4</sub> prepared by sol-gel auto-combustion shows good sensitivity to ethanol and methanol. It was observed that for doped ferrites, sensitivity was higher than for undoped one. Doping help in reducing both response times as well as working temperature. The gas sensor aim at developing material with high sensitivity and selective long term devices. With increased development in technology, demand to develop a high quality ferrite as gas sensor will arise. As a result other applications of ferrites will be discovered.

## References

- Kapse, V. D. Preparation of Nanocrystalline Spinel-Type Oxide Materials for Gas Sensing Applications. *Res. J. Chem. Sci.* 2015, 5, 7–12.
- Smulko, J. M.; Trawka, M.; Granqvist, C. G.; Ionescu, R.; Annanouch, F.; Llobet, E.; Kish, L. B. New Approaches for Improving Selectivity and Sensitivity of Resistive Gas Sensors: A Review. *Sens. Rev.* 2015, 35, 340–347. doi:10.1108/SR-12-2014-0747
- Sberveglieri, G. (Ed.). *Gas Sensors: principles, Operation and Developments*; Berlin, Germany: Springer Science & Business Media, 2012.
- Symons, E. A. Catalytic Gas Sensors. In *Gas Sensors*; Springer: Dordrecht, 1992; pp 169–185.
- Bakker, E.; Telting-Diaz, M. Electrochemical Sensors. *Anal. Chem.* 2002, 74, 2781–2800. doi:10.1021/ac0202278
- Hodgkinson, J.; Tatam, R. P. Optical Gas Sensing: A Review. *Meas. Sci. Technol.* 2013, 24, 012004. doi:10.1088/0957-0233/24/1/012004
- Bhattacharyya, P. Technological Journey towards Reliable Microheater Development for MEMS Gas Sensors: A Review. *IEEE Trans. Device Mater. Reliab.* 2014, 14, 589–599. doi:10.1109/TDMR.2014.2311801
- Cheeke, J. D. N.; Wang, Z. Acoustic Wave Gas Sensors. *Sens. Actuators B.* 1999, 59, 146–153. doi:10.1016/S0925-4005(99)00212-9
- Jakubik, W. P. Surface Acoustic Wave-Based Gas Sensors. *Thin Solid Films* 2011, 520, 986–993. doi:10.1016/j.tsf.2011.04.174
- Meixner, H.; Lampe, U. Metal Oxide Sensors. *Sens. Actuators B.* 1996, 33, 198–202. doi:10.1016/0925-4005(96)80098-0
- Patil, D.; Patil, V.; Patil, P. Highly Sensitive and Selective LPG Sensor Based on  $\alpha$ -Fe<sub>2</sub>O<sub>3</sub> Nanorods. *Sens. Actuators B.* 2011, 152, 299–306. doi:10.1016/j.snb.2010.12.025
- Kapse, V. D.; Ghosh, S. A.; Raghuvanshi, F. C.; Kapse, S. D. Nanocrystalline Spinel Ni<sub>0.6</sub>Zn<sub>0.4</sub>Fe<sub>2</sub>O<sub>4</sub>: A Novel Material for H<sub>2</sub>S Sensing. *Mater. Chem. Phys.* 2009, 113, 638–644. doi:10.1016/j.matchemphys.2008.08.017
- Mukherjee, K.; Majumder, S. B. Reducing Gas Sensing Behavior of Nano-Crystalline Magnesium-Zinc Ferrite Powders. *Talanta* 2010, 81, 1826–1832. doi:10.1016/j.talanta.2010.03.042
- Chu, X. F.; Liu, X. Q.; Meng, G. Y. The Catalytic Effect of SmInO<sub>3</sub> on the Gas-Sensing Properties of Cd<sub>2</sub>O<sub>4</sub>. *Mater. Sci. Eng. B.* 1999, 64, 60–63.
- Ngoc, T. M.; Van Duy, N.; Hoa, N. D.; Hung, C. M.; Nguyen, H.; Van Hieu, N. Effective Design and Fabrication of Low-Power-Consumption Self-Heated SnO<sub>2</sub> Nanowire Sensors for Reducing Gases. *Sens. Actuators B.* 2019, 295, 144–152. doi:10.1016/j.snb.2019.05.074
- Barsan, N.; Schweizer-Berberich, M.; Göpel, W. Fundamental and Practical Aspects in the Design of Nanoscaled SnO<sub>2</sub> Gas Sensors: A Status Report. *Fresenius' J. Anal. Chem.* 1999, 365, 287–304. doi:10.1007/s002160051490
- Tyagi, P.; Sharma, A.; Tomar, M.; Gupta, V. Metal Oxide Catalyst Assisted SnO<sub>2</sub> Thin Film Based SO<sub>2</sub> Gas Sensor. *Sens. Actuators B.* 2016, 224, 282–289. doi:10.1016/j.snb.2015.10.050
- Chou, S. M.; Teoh, L. G.; Lai, W. H.; Su, Y. H.; Hon, M. H. ZnO: Al Thin Film Gas Sensor for Detection of Ethanol Vapor. *Sensors.* 2006, 6, 1420–1427. doi:10.3390/s6101420
- Sadek, A. Z.; Choopun, S.; Wlodarski, W.; Ippolito, S. J.; Kalantar-Zadeh, K. Characterization of ZnO Nanobelt-Based Gas Sensor for H<sub>2</sub>S, NO<sub>2</sub> and Hydrocarbon Sensing. *IEEE Sens. J.* 2007, 7, 919–924. doi:10.1109/JSEN.2007.895963
- Hjiri, M.; Dhahri, R.; Omri, K.; El Mir, L.; Leonardi, S. G.; Donato, N.; Neri, G. Effect of Indium Doping on ZnO Based-Gas Sensor for CO. *Mater. Sci. Semicond. Process.* 2014, 27, 319–325. doi:10.1016/j.mssp.2014.07.009
- Penza, M.; Tagliente, M. A.; Mirengi, L.; Gerardi, C.; Martucci, C.; Cassano, G. Tungsten Trioxide (WO<sub>3</sub>) Sputtered Thin Films for a NO<sub>x</sub> Gas Sensor. *Sens. Actuators B.* 1998, 50, 9–18. doi:10.1016/S0925-4005(98)00149-X
- Zeng, J.; Hu, M.; Wang, W.; Chen, H.; Qin, Y. NO<sub>2</sub>-Sensing Properties of Porous WO<sub>3</sub> Gas Sensor Based on Anodized Sputtered Tungsten Thin Film. *Sens. Actuators B.* 2012, 161, 447–452. doi:10.1016/j.snb.2011.10.059
- Van Uitert, L. D. Dc Resistivity in the Nickel and Nickel Zinc Ferrite System. *J. Chem. Phys.* 1955, 23, 1883–1887. doi:10.1063/1.1740598
- Barsan, N.; Weimar, U. Conduction Model of Metal Oxide Gas Sensors. *J. Electroceram.* 2001, 7, 143–167. doi:10.1023/A:1014405811371
- Rezlescu, N.; Doroftei, C.; Rezlescu, E.; Popa, P. Lithium Ferrite for Gas Sensing Applications. *Sens. Actuators B.* 2008, 133, 420–425. doi:10.1016/j.snb.2008.02.047
- Sun, Z.; Liu, L.; Zeng Jia, D.; Pan, W. Simple Synthesis of CuFe<sub>2</sub>O<sub>4</sub> Nanoparticles as Gas-Sensing Materials. *Sens. Actuators B.* 2007, 125, 144–148. doi:10.1016/j.snb.2007.01.050
- Wang, C.; Yin, L.; Zhang, L.; Xiang, D.; Gao, R. Metal Oxide Gas Sensors: Sensitivity and Influencing Factors. *Sensors (Basel).* 2010, 10, 2088–2106. doi:10.3390/s100302088
- Mohammadi, M. R.; Fray, D. J.; Ghorbani, M. Comparison of Single and Binary Oxide Sol-Gel Gas

- Sensors Based on Titania. *Solid State Sci.* 2008, 10, 884–893. doi:10.1016/j.solidstatesciences.2007.10.035
29. Galatsis, K.; Li, Y. X.; Wlodarski, W.; Comini, E.; Sberveglieri, G.; Cantalini, C.; Santucci, S.; Passacantando, M. Comparison of Single and Binary Oxide MoO<sub>3</sub>, TiO<sub>2</sub> and WO<sub>3</sub> Sol–Gel Gas Sensors. *Sens. Actuators B.* 2002, 83, 276–280. doi:10.1016/S0925-4005(01)01072-3
  30. Nakate, U. T.; Patil, P.; Nakate, Y. T.; Na, S. I.; Yu, Y. T.; Hahn, Y. B. Ultrathin Ternary Metal Oxide Bi<sub>2</sub>MoO<sub>6</sub> Nanosheets for High Performance Asymmetric Supercapacitor and Gas Sensor Applications. *Appl. Surf. Sci.* 2021, 551, 149422. doi:10.1016/j.apsusc.2021.149422
  31. Rai, P.; Majhi, S. M.; Yu, Y. T.; Lee, J. H. Noble Metal@ Metal Oxide Semiconductor Core@ Shell Nano-Architectures as a New Platform for Gas Sensor Applications. *RSC Adv.* 2015, 5, 76229–76248. doi:10.1039/C5RA14322E
  32. Zhou, L.; Bai, J.; Liu, Y.; Liu, F.; Wang, H.; Zhang, Y.; Lu, G. Highly Sensitive C<sub>2</sub>H<sub>2</sub> Gas Sensor Based on Ag Modified ZnO Nanorods. *Ceram. Int.* 2020, 46, 15764–15771. doi:10.1016/j.ceramint.2020.03.120
  33. Cabot, A.; Arbiol, J.; Morante, J. R.; Weimar, U.; Barsan, N.; Göpel, W. Analysis of the Noble Metal Catalytic Additives Introduced by Impregnation of as Obtained SnO<sub>2</sub> Sol–Gel Nanocrystals for Gas Sensors. *Sens. Actuators B.* 2000, 70, 87–100. doi:10.1016/S0925-4005(00)00565-7
  34. Cheng, P.; Wang, Y.; Wang, C.; Ma, J.; Xu, L.; Lv, C.; Sun, Y. Investigation about Doping Effects of Different Noble Metals for Ethanol Gas Sensors Based on Mesoporous In<sub>2</sub>O<sub>3</sub>. *Nanotechnology.* 2021, 32, 305503. doi:10.1088/1361-6528/abf453
  35. Hou, L.; Zhang, C.; Li, L.; Du, C.; Li, X.; Kang, X. F.; Chen, W. CO Gas Sensors Based on p-Type CuO Nanotubes and CuO Nanocubes: Morphology and Surface Structure Effects on the Sensing Performance. *Talanta.* 2018, 188, 41–49. doi:10.1016/j.talanta.2018.05.059
  36. Gustafson, J. A.; Wilmer, C. E. Computational Design of Metal–Organic Framework Arrays for Gas Sensing: Influence of Array Size and Composition on Sensor Performance. *J. Phys. Chem. C.* 2017, 121, 6033–6038. doi:10.1021/acs.jpcc.6b09740
  37. Zhou, X.; Cheng, X.; Zhu, Y.; Elzatahry, A. A.; Alghamdi, A.; Deng, Y.; Zhao, D. Ordered Porous Metal Oxide Semiconductors for Gas Sensing. *Chin. Chem. Lett.* 2018, 29, 405–416. doi:10.1016/j.ccllet.2017.06.021
  38. Zhang, J.; Lu, H.; Liu, C.; Chen, C.; Xin, X. Porous NiO–WO<sub>3</sub> Heterojunction Nanofibers Fabricated by Electrospinning with Enhanced Gas Sensing Properties. *RSC Adv.* 2017, 7, 40499–40509. doi:10.1039/C7RA07663K
  39. Xu, T.; Pei, Y.; Liu, Y.; Wu, D.; Shi, Z.; Xu, J.; Tian, Y.; Li, X. High-Response NO<sub>2</sub> Resistive Gas Sensor Based on Bilayer MoS<sub>2</sub> Grown by a New Two-Step Chemical Vapor Deposition Method. *J. Alloys Compd.* 2017, 725, 253–259. doi:10.1016/j.jallcom.2017.06.105
  40. Gui, Y.; Tian, K.; Liu, J.; Yang, L.; Zhang, H.; Wang, Y. Superior Triethylamine Detection at Room Temperature by {–112} Faceted WO<sub>3</sub> Gas Sensor. *J. Hazard. Mater.* 2019, 380, 120876. doi:10.1016/j.jhazmat.2019.120876
  41. Duan, X.; Chen, G.; Gao, P.; Jin, W.; Ma, X.; Yin, Y.; Guo, L.; Ye, H.; Zhu, Y.; Yu, J.; Wu, Y. Crystallography Facet Tailoring of Carbon Doped ZnO Nanorods via Selective Etching. *Appl. Surf. Sci.* 2017, 406, 186–191. doi:10.1016/j.apsusc.2017.02.119
  42. Falsafi, F.; Hashemi, B.; Mirzaei, A.; Fazio, E.; Neri, F.; Donato, N.; Leonardi, S. G.; Neri, G. Sm-Doped Cobalt Ferrite Nanoparticles: A Novel Sensing Material for Conductometric Hydrogen Leak Sensor. *Ceram. Int.* 2017, 43, 1029–1037. doi:10.1016/j.ceramint.2016.10.035
  43. Kim, H.; Pak, Y.; Jeong, Y.; Kim, W.; Kim, J.; Jung, G. Y. Amorphous Pd-Assisted H<sub>2</sub> Detection of ZnO Nanorod Gas Sensor with Enhanced Sensitivity and Stability. *Sens. Actuators B.* 2018, 262, 460–468. doi:10.1016/j.snb.2018.02.025
  44. Ponzoni, A.; Baratto, C.; Cattabiani, N.; Falasconi, M.; Galstyan, V.; Nunez-Carmona, E.; Rigoni, F.; Sberveglieri, V.; Zambotti, G.; Zappa, D. Metal Oxide Gas Sensors, a Survey of Selectivity Issues Addressed at the Sensor Lab, Brescia (Italy). *Sensors.* 2017, 17, 714. doi:10.3390/s17040714
  45. Tudorache, F.; Popa, P. D.; Dobromir, M.; Iacomì, F. Studies on the Structure and Gas Sensing Properties of Nickel–Cobalt Ferrite Thin Films Prepared by Spin Coating. *Mater. Sci. Eng. B.* 2013, 178, 1334–1338. doi:10.1016/j.mseb.2013.03.019
  46. Issa, B.; Obaidat, I. M.; Albiss, B. A.; Haik, Y. Magnetic Nanoparticles: Surface Effects and Properties Related to Biomedicine Applications. *Int. J. Mol. Sci.* 2013, 14, 21266–21305. doi:10.3390/ijms141121266
  47. Sutka, A.; Mezinskis, G. Sol-Gel Auto-Combustion Synthesis of Spinel-Type Ferrite Nanomaterials. *Front. Mater. Sci.* 2012, 6, 128–141. doi:10.1007/s11706-012-0167-3
  48. Singh, S.; Singh, A.; Yadav, R. R.; Tandon, P. Growth of Zinc Ferrite Aligned Nanorods for Liquefied Petroleum Gas Sensing. *Mater. Lett.* 2014, 131, 31–34. doi:10.1016/j.matlet.2014.05.167
  49. Leroux, C.; Bendahan, M.; Madigou, V.; Ajroudi, L.; Mliki, N. Nanoparticles of Cobalt Ferrite for NH<sub>3</sub> Sensing. *Sens. Transducers.* 2014, 27, 239.
  50. Sharma, R.; & Sharma, V. Structural, Morphological and Magnetic Studies of Transition Metal Doped Mg–Zn Ferrites; 2019.
  51. Kamble, R. B.; Mathe, V. L. Nanocrystalline Nickel Ferrite Thick Film as an Efficient Gas Sensor at Room Temperature. *Sens. Actuators B.* 2008, 131, 205–209. doi:10.1016/j.snb.2007.11.003
  52. Singh, S.; Verma, N.; Yadav, B. C.; Prakash, R. A Comparative Study on Surface Morphological Investigations of Ferric Oxide for LPG and Opto-Electronic Humidity Sensors. *Appl. Surf. Sci.* 2012, 258, 8780–8789. doi:10.1016/j.apsusc.2012.05.091



53. Gadkari, A. B.; Shinde, T. J.; Vasambekar, P. N. Ferrite Gas Sensors. *IEEE Sens. J.* 2011, 11, 849–861. doi:10.1109/JSEN.2010.2068285
54. Srivastava, R.; Yadav, B. C. Ferrite Materials: introduction, Synthesis Techniques, and Applications as Sensors. *Int. J. Green Nanotechnol.* 2012, 4, 141–154. doi:10.1080/19430892.2012.676918
55. Joshi, S.; Kamble, V. B.; Kumar, M.; Umarji, A. M.; Srivastava, G. Nickel Substitution Induced Effects on Gas Sensing Properties of Cobalt Ferrite Nanoparticles. *J. Alloys Compd.* 2016, 654, 460–466. doi:10.1016/j.jallcom.2015.09.119
56. Yadav, A. K.; Singh, R. K.; Singh, P. Fabrication of Lanthanum Ferrite Based Liquefied Petroleum Gas Sensor. *Sens. Actuators B.* 2016, 229, 25–30. doi:10.1016/j.snb.2016.01.066
57. Yang, X.; Zhang, S.; Yu, Q.; Sun, P.; Liu, F.; Lu, H.; Yan, X.; Zhou, X.; Liang, X.; Gao, Y.; Lu, G. Solvothermal Synthesis of Porous  $\text{CuFe}_2\text{O}_4$  Nanospheres for High Performance Acetone Sensor. *Sens. Actuators B.* 2018, 270, 538–544. doi:10.1016/j.snb.2018.05.078
58. Doroftei, C.; Prelipceanu, O. S.; Carlescu, A.; Leontie, L.; Prelipceanu, M. 2018 Porous Spinel-Type Oxide Semiconductors for High-Performance Acetone Sensors. In 2018 International Conference on Development and Application Systems (DAS) (pp. 110–113). IEEE. doi:10.1109/DAAS.2018.8396081
59. Wang, X. F.; Sun, K. M.; Li, S. J.; Song, X. Z.; Cheng, L.; Ma, W. Porous Javelin-like  $\text{NiFe}_2\text{O}_4$  Nanorods as n-Propanol Sensor with Ultrahigh-Performance. *ChemistrySelect.* 2018, 3, 12871–12877. doi:10.1002/slct.201802879
60. Li, F.; Guo, S.; Shen, J.; Shen, L.; Sun, D.; Wang, B.; Chen, Y.; Ruan, S. Xylene Gas Sensor Based on Au-Loaded  $\text{WO}_3\text{-H}_2\text{O}$  Nanocubes with Enhanced Sensing Performance. *Sens. Actuators B.* 2017, 238, 364–373. doi:10.1016/j.snb.2016.07.021
61. Yang, X.; Li, H.; Li, T.; Li, Z.; Wu, W.; Zhou, C.; Sun, P.; Liu, F.; Yan, X.; Gao, Y.; et al. Highly Efficient Ethanol Gas Sensor Based on Hierarchical  $\text{SnO}_2/\text{Zn}_2\text{SnO}_4$  Porous Spheres. *Sens. Actuators B.* 2019, 282, 339–346. doi:10.1016/j.snb.2018.11.070
62. Choi, Y. H.; Kim, D. H.; Hong, S. H. Gas Sensing Properties of p-Type  $\text{CuBi}_2\text{O}_4$  Porous Nanoparticulate Thin Film Prepared by Solution Process Based on Metal-Organic Decomposition. *Sens. Actuators B.* 2018, 268, 129–135. doi:10.1016/j.snb.2018.04.105
63. Xu, Y.; Tian, X.; Liu, P.; Sun, Y.; Du, G.  $\text{GIn}_2\text{O}_3$  Nanoplates with Different Crystallinity and Porosity: Controllable Synthesis and Gas-Sensing Properties Investigation. *J. Alloys Compd.* 2019, 787, 1063–1073. doi:10.1016/j.jallcom.2019.02.176
64. Umar, A.; Hahn, Y. B., Eds. *Metal Oxide Nanostructures and Their Applications*; American Scientific Publishers, USA, 2010; Vol. 3.
65. Rezlescu, N.; Doroftei, C.; Popa, P. D. Humidity-Sensitive Electrical Resistivity of  $\text{MgFe}_2\text{O}_4$  and  $\text{Mg}_{0.9}\text{Sn}_{0.1}\text{Fe}_2\text{O}_4$  Porous Ceramics. *Rom. J. Phys.* 2007, 52, 353.
66. Cao, Y.; Qin, H.; Niu, X.; Jia, D. Simple Solid-State Chemical Synthesis and Gas-Sensing Properties of Spinel Ferrite Materials with Different Morphologies. *Ceram. Int.* 2016, 42, 10697–10703. doi:10.1016/j.ceramint.2016.03.184
67. Scherrer, P. Bestimmung Der Grösse Und Der Inneren Von Kolloidteilchen Mittels Röntgenstrahlen Struktur Nachr. Ges. Wiss. Göttingen. 1918, 26, 98–100.
68. Langford, J. I.; Wilson, A. J. C. Scherrer after Sixty Years: A Survey and Some New Results in the Determination of Crystallite Size. *J. Appl. Crystallogr.* 1978, 11, 102–113. doi:10.1107/S0021889878012844
69. Kril, C. E.; Birringer, R. Estimating Grain-Size Distributions in Nanocrystalline Materials from X-Ray Diffraction Profile Analysis. *Philos. Mag. A.* 1998, 77, 621–640. doi:10.1080/01418619808224072
70. Ares, J. R.; Pascual, A.; Ferrer, I. J.; Sánchez, C. Grain and Crystallite Size in Polycrystalline Pyrite Thin Films. *Thin Solid Films.* 2005, 480–481, 477–481. doi:10.1016/j.tsf.2004.11.064
71. Jones, F. W. The Measurement of Particle Size by the X-Ray Method. *Proc. R. Soc. Lond. A.* 1938, 166, 16–43.
72. Chen, N.S.; Yang, X. J.; Liu, E. S.; Huang, J. L. Reducing Gas-Sensing Properties of Ferrite Compounds  $\text{MFe}_2\text{O}_4$  ( $\text{M}=\text{Cu, Zn, Cd}$  and  $\text{Mg}$ ). *Sens. Actuators B.* 2000, 66, 178–180. doi:10.1016/S0925-4005(00)00368-3
73. Verma, A.; Thakur, O. P.; Prakash, C.; Goel, T. C.; Mendiratta, R. G. Temperature Dependence of Electrical Properties of Nickel-Zinc Ferrites Processed by the Citrate Precursor Technique. *Mater. Sci. Eng. B.* 2005, 116, 1–6. doi:10.1016/j.mseb.2004.08.011
74. Watawe, S. C.; Sarwade, B. D.; Bellad, S. S.; Sutar, B. D.; Chougule, B. K. Microstructure, Frequency and Temperature-Dependent Dielectric Properties of Cobalt-Substituted Lithium Ferrites. *J. Magn. Magn. Mater.* 2000, 214, 55–60. doi:10.1016/S0304-8853(00)00033-0
75. Mandal, S. K.; Singh, S.; Dey, P.; Roy, J. N.; Mandal, P. R.; Nath, T. K. Temperature and Frequency Dependence of AC Electrical Properties of Zn and Ni Doped  $\text{CoFe}_2\text{O}_4$  Nanocrystals. *Philos. Mag.* 2017, 97, 1628–1645. doi:10.1080/14786435.2017.1312021
76. Jadhav, P.; Patankar, K.; Mathe, V.; Tarwal, N. L.; Jang, J. H.; Puri, V. Structural and Magnetic Properties of  $\text{Ni}_{0.8}\text{Co}_{0.2-2x}\text{Cu}_x\text{Mn}_x\text{Fe}_2\text{O}_4$  Spinel Ferrites Prepared via Solution Combustion Route. *J. Magn. Magn. Mater.* 2015, 385, 160–165. doi:10.1016/j.jmmm.2015.03.020
77. Hench, L. L.; West, J. K. *Principles of Electronic Ceramics*; John Wiley and Sons: New York, 1990; 1989.
78. Tudorache, F.; Rezlescu, E.; Popa, P. D.; Rezlescu, N. Study of Some Simple Ferrites as Reducing Gas Sensors. *J. Optoelectron. Adv. Mater.* 2008, 10, 1889–1893.
79. Satyanarayana, L.; Reddy, K. M.; Manorama, S. V. Synthesis of Nanocrystalline  $\text{Ni}_{1-x}\text{Co}_x\text{Mn}_x\text{Fe}_2\text{O}_4$ : A Material for Liquefied Petroleum Gas Sensing. *Sens.*

- Actuators B.* 2003, 89, 62–67. doi:10.1016/S0925-4005(02)00429-X
80. Dey, A. Semiconductor Metal Oxide Gas Sensors: A Review. *Mater. Sci. Eng. B.* 2018, 229, 206–217. doi: 10.1016/j.mseb.2017.12.036
  81. Rezlescu, N.; Rezlescu, E.; Tudorache, F.; Popa, P. D. Gas Sensing Properties of Porous Cu-, Cd- and Zn-Ferrites. *Rom. Rep. Phys.* 2009, 61, 223–234.
  82. Zhang, P.; Qin, H.; Lv, W.; Zhang, H.; Hu, J. Gas Sensors Based on Ytterbium Ferrites Nanocrystalline Powders for Detecting Acetone with Low Concentrations. *Sens. Actuators B.* 2017, 246, 9–19. doi:10.1016/j.snb.2017.01.096
  83. Kumar, E. R.; Reddy, P. S. P.; Devi, G. S.; Sathiyaraj, S. Structural, Dielectric and Gas Sensing Behaviour of Mn Substituted Spinel  $MFe_2O_4$  ( $M = Zn, Cu, Ni$ , and  $Co$ ) Ferrite Nanoparticles. *J. Magn. Magn. Mater.* 2016, 398, 281–288. doi:10.1016/j.jmmm.2015.09.018
  84. Rajamallu, K. Synthesis and Gas Sensitivity Properties of Ferrites ( $MFe_2O_4$ ;  $M = Zn, Ni$  and  $Co$ ) Nanoparticles; 2018.
  85. Poghosian, A. S.; Abovian, H. V.; Avakian, P. B.; Mkrtchian, S. H.; Haroutunian, V. M. Bismuth Ferrites: New Materials for Semiconductor Gas Sensors. *Sens. Actuators B.* 1991, 4, 545–549. doi:10.1016/0925-4005(91)80167-I
  86. Wetchakun, K.; Samerjai, T.; Tamaekong, N.; Liewhiran, C.; Siriwong, C.; Kruefu, V.; Wisitsoraat, A.; Tuantranont, A.; Phanichphant, S. Semiconducting Metal Oxides as Sensors for Environmentally Hazardous Gases. *Sens. Actuators B.* 2011, 160, 580–591. doi:10.1016/j.snb.2011.08.032
  87. Wu, J.; Gao, D.; Sun, T.; Bi, J.; Zhao, Y.; Ning, Z.; Fan, G.; Xie, Z. Highly Selective Gas Sensing Properties of Partially Inversed Spinel Zinc Ferrite towards  $H_2S$ . *Sens. Actuators B.* 2016, 235, 258–262. doi:10.1016/j.snb.2016.05.083
  88. Tumberphale, U. B.; Jadhav, S. S.; Raut, S. D.; Shinde, P. V.; Sangle, S.; Shaikh, S. F.; Al-Enizi, A. M.; Ubaidullah, M.; Mane, R. S.; Gore, S. K. Tailoring Ammonia Gas Sensing Performance of  $La^{3+}$ -Doped Copper Cadmium Ferrite Nanostructures. *Solid State Sci.* 2020, 100, 106089. doi:10.1016/j.solidstatesciences.2019.106089
  89. Yang, W.; Gan, L.; Li, H.; Zhai, T. Two-Dimensional Layered Nanomaterials for Gas-Sensing Applications. *Inorg. Chem. Front.* 2016, 3, 433–451. doi:10.1039/C5QI00251F
  90. Singh, A.; Singh, A.; Singh, S.; Tandon, P.; Yadav, B. C. Preparation and Characterization of Nanocrystalline Nickel Ferrite Thin Films for Development of a Gas Sensor at Room Temperature. *J. Mater. Sci. Mater. Electron.* 2016, 27, 8047–8054. doi:10.1007/s10854-016-4802-0
  91. Kadu, A. V.; Jagtap, S. V.; Chaudhari, G. Studies on the Preparation and Ethanol Gas Sensing Properties of Spinel  $Ni_{0.6}Zn_{0.4}Fe_2O_4$  Nanomaterials. *Curr. Appl. Phys.* 2009, 9, 1246–1251. doi:10.1016/j.cap.2009.02.001
  92. Pathania, A.; Thakur, P.; Tomar, M.; Gupta, V.; Trukhanov, A. V.; Trukhanov, S. V.; Thakur, A. Development of Tungsten Doped Ni-Zn Nano-Ferrites with Fast Response and Recovery Time for Hydrogen Gas Sensing Application. *Results Phys.* 2019, 15, 102531.
  93. Gadkari, A. B.; Shinde, T. J.; Vasambekar, P. N. Effect of  $Sm^{3+}$  Ion Addition on Gas Sensing Properties of  $Mg_{1-x}Cd_xFe_2O_4$  System. *Sens. Actuators B.* 2013, 178, 34–39. doi:10.1016/j.snb.2012.12.023
  94. Reddy, C. G.; Manorama, S. V.; Rao, V. J. Semiconducting Gas Sensor for Chlorine Based on Inverse Spinel Nickel Ferrite. *Sens. Actuators B.* 1999, 55, 90–95.
  95. Korotcenkov, G. Metal Oxides for Solid-State Gas Sensors: What Determines Our Choice? *Mater. Sci. Eng. B.* 2007, 139, 1–23. doi:10.1016/j.mseb.2007.01.044
  96. Abu-Hani, A. F.; Mahmoud, S. T.; Awwad, F.; Ayesh, A. I. Design, Fabrication, and Characterization of Portable Gas Sensors Based on Spinel Ferrite Nanoparticles Embedded in Organic Membranes. *Sens. Actuators B.* 2017, 241, 1179–1187. doi:10.1016/j.snb.2016.10.016
  97. Mukherjee, K.; Majumder, S. B. Analyses of Response and Recovery Kinetics of Zinc Ferrite as Hydrogen Gas Sensor. *J. Appl. Phys.* 2009, 106, 064912. doi:10.1063/1.3225996
  98. Rezlescu, N.; Iftimie, N.; Rezlescu, E.; Doroftei, C.; Popa, P. D. Semiconducting Gas Sensor for Acetone Based on the Fine Grained Nickel Ferrite. *Sens. Actuators B.* 2006, 114, 427–432. doi:10.1016/j.snb.2005.05.030
  99. Darshane, S. L.; Suryavanshi, S. S.; Mulla, I. S. Nanostructured Nickel Ferrite: A Liquid Petroleum Gas Sensor. *Ceram. Int.* 2009, 35, 1793–1797. doi:10.1016/j.ceramint.2008.10.013
  100. Zhang, Y. M.; Lin, Y. T.; Chen, J. L.; Zhang, J.; Zhu, Z. Q.; Liu, Q. J. A High Sensitivity Gas Sensor for Formaldehyde Based on Silver Doped Lanthanum Ferrite. *Sens. Actuators B.* 2014, 190, 171–176. doi: 10.1016/j.snb.2013.08.046
  101. Mukherjee, K.; Majumder, S. B. Analyses of Conductance Transients to Address the Selectivity Issue of Zinc Ferrite Gas Sensors. *Electrochem. Solid-State Lett.* 2010, 13, J25. doi:10.1149/1.3290743
  102. Nemov, T. G.; Yordanov, S. P. *Ceramic Sensors—Technology and Application*; Technomic Publishing Company Inc: Lancaster, PA, 1996; Vol. 138, pp 703–708.
  103. Singh, M.; Yadav, B. C.; Ranjan, A.; Sonker, R. K.; Kaur, M. Detection of Liquefied Petroleum Gas below Lowest Explosion Limit (LEL) Using Nanostructured Hexagonal Strontium Ferrite Thin Film. *Sens. Actuators B.* 2017, 249, 96–104. doi:10.1016/j.snb.2017.04.075
  104. Singh, A.; Singh, A.; Singh, S.; Tandon, P.; Yadav, B. C.; Yadav, R. R. Synthesis, Characterization and Performance of Zinc Ferrite Nanorods for Room Temperature Sensing Applications. *J. Alloys Compd.* 2015, 618, 475–483. doi:10.1016/j.jallcom.2014.08.190
  105. Li, L.; Tan, J.; Dun, M.; Huang, X. Porous  $ZnFe_2O_4$  Nanorods with Net-Worked Nanostructure for

- Highly Sensor Response and Fast Response Acetone Gas Sensor. *Sens. Actuators B*. 2017a, 248, 85–91. doi:10.1016/j.snb.2017.03.119
106. Zhang, D.; Jiang, C.; Wu, J. Layer-by-Layer Assembled  $\text{In}_2\text{O}_3$  Nanocubes/Flower-Like  $\text{MoS}_2$  Nanofilm for Room Temperature Formaldehyde Sensing. *Sens. Actuators B*. 2018, 273, 176–184. doi:10.1016/j.snb.2018.06.044
107. Boulmani, R.; Bendahan, M.; Lambert-Mauriat, C.; Gillet, M.; Aguir, K. Correlation between rf-Sputtering Parameters and  $\text{WO}_3$  Sensor Response towards Ozone. *Sens. Actuators B*. 2007, 125, 622–627. doi:10.1016/j.snb.2007.03.011
108. Kanu, S. S.; Binions, R. Thin Films for Solar Control Applications. *Proc. R Soc. A*. 2010, 466, 19–44. doi:10.1098/rspa.2009.0259
109. Cerda, J.; Cirera, A.; Vila, A.; Cornet, A.; Morante, J. R. Deposition on Micromachined Silicon Substrates of Gas Sensitive Layers Obtained by a Wet Chemical Route: A  $\text{CO}/\text{CH}_4$  High Performance Sensor. *Thin Solid Films*. 2001, 391, 265–269. doi:10.1016/S0040-6090(01)00993-2
110. Gardon, M.; Guilemany, J. M. A Review on Fabrication, Sensing Mechanisms and Performance of Metal Oxide Gas Sensors. *J. Mater. Sci. Mater. Electron*. 2013, 24, 1410–1421. doi:10.1007/s10854-012-0974-4
111. Reddy, C. G.; Manorama, S. V.; Rao, V. J. Preparation and Characterization of Ferrites as Gas Sensor Materials. *J. Mater. Sci. Lett*. 2000, 19, 775–778. doi:10.1023/A:1006716721984
112. Tsai, C. J.; Yang, C. Y.; Liao, Y. C.; Chueh, Y. L. Hydrothermally Grown Bismuth Ferrites: Controllable Phases and Morphologies in a Mixed  $\text{KOH}/\text{NaOH}$  Mineralizer. *J. Mater. Chem*. 2012, 22, 17432–17436. doi:10.1039/c2jm33859a
113. Chen, C.; Cheng, J.; Yu, S.; Che, L.; Meng, Z. Hydrothermal Synthesis of Perovskite Bismuth Ferrite Crystallites. *J. Cryst. Growth*. 2006, 291, 135–139. doi:10.1016/j.jcrysgro.2006.02.048
114. Patil, J. Y.; Khandekar, M. S.; Mulla, I. S.; Suryavanshi, S. S. Combustion Synthesis of Magnesium Ferrite as Liquid Petroleum Gas (LPG) Sensor: Effect of Sintering Temperature. *Curr. Appl. Phys*. 2012, 12, 319–324. doi:10.1016/j.cap.2011.06.029
115. Mukherjee, K.; Majumder, S. B. Synthesis Process Induced Improvement on the Gas Sensing Characteristics of Nano-Crystalline Magnesium Zinc Ferrite Particles. *Sens. Actuators B*. 2012, 162, 229–236. doi:10.1016/j.snb.2011.12.072
116. Tao, S.; Gao, F.; Liu, X.; Sørensen, O. T. Preparation and Gas-Sensing Properties of  $\text{CuFe}_2\text{O}_4$  at Reduced Temperature. *Mater. Sci. Eng. B*. 2000, 77, 172–176. doi:10.1016/S0921-5107(00)00473-6
117. Oura, K.; Katayama, M.; Zotov, A. V.; Lifshits, V. G.; Saranin, A. A. Elementary Processes at Surfaces II. Surface Diffusion. In *Surface Science*; Springer: Berlin, Heidelberg, 2003; pp 325–356.
118. Jiao, Z.; Wu, M.; Gu, J.; Qin, Z. Preparation and Gas-Sensing Characteristics of Nanocrystalline Spinel Zinc Ferrite Thin Films. *IEEE Sens. J*. 2003, 3, 435–438.
119. Patil, J. Y.; Nadargi, D. Y.; Gurav, J. L.; Mulla, I. S.; Suryavanshi, S. S. Synthesis of Glycine Combusted  $\text{NiFe}_2\text{O}_4$  Spinel Ferrite: A Highly Versatile Gas Sensor. *Mater. Lett*. 2014, 124, 144–147. doi:10.1016/j.matlet.2014.03.051
120. Park, C. O.; Akbar, S. A. Ceramics for Chemical Sensing. *J. Mater. Sci*. 2003, 38, 4611–4637. doi:10.1023/A:1027402430153
121. Yamazoe, N. New Approaches for Improving Semiconductor Gas Sensors. *Sens. Actuators B*. 1991, 5, 7–19. doi:10.1016/0925-4005(91)80213-4
122. Yamazoe, N.; Sakai, G.; Shimano, K. Oxide Semiconductor Gas Sensors. *Catal. Surv. Asia* 2003, 7, 63–75. doi:10.1023/A:1023436725457
123. Hankare, P. P.; Jadhav, S. D.; Sankpal, U. B.; Patil, R. P.; Sasikala, R.; Mulla, I. Gas Sensing Properties of Magnesium Ferrite Prepared by Co-precipitation Method. *J. Alloys Compd*. 2009, 488, 270–272. doi:10.1016/j.jallcom.2009.08.103
124. Sugimoto, M. The past, Present, and Future of Ferrites. *J. Am. Ceram. Soc*. 2004, 82, 269–280. doi:10.1111/j.1551-2916.1999.tb20058.x
125. Fazio, E.; Spadaro, S.; Corsaro, C.; Neri, G.; Leonardi, S. G.; Neri, F.; Lavanya, N.; Sekar, C.; Donato, N.; Neri, G. Metal-Oxide Based Nanomaterials: Synthesis, Characterization and Their Applications in Electrical and Electrochemical Sensors. *Sensors*. 2021, 21, 2494. doi:10.3390/s21072494
126. Yamazoe, N.; Miura, N. Development of Gas Sensors for Environmental Protection. *IEEE Trans. Comp, Packag, Manufact. Technol. A*. 1995, 18, 252–256. doi:10.1109/95.390298
127. Lantto, V.; Romppainen, P. Electrical Studies on the Reactions of CO with Different Oxygen Species on  $\text{SnO}_2$  Surfaces. *Surf. Sci*. 1987, 192, 243–264. doi:10.1016/S0039-6028(87)81174-3
128. Kim, H. J.; Lee, J. H. Highly Sensitive and Selective Gas Sensors Using p-Type Oxide Semiconductors: Overview. *Sens. Actuators B*. 2014, 192, 607–627. doi:10.1016/j.snb.2013.11.005
129. Mukherjee, C.; Mondal, R.; Dey, S.; Kumar, S.; Das, J. Nanocrystalline Copper Nickel Zinc Ferrite: Efficient Sensing Materials for Ethanol and Acetone at Room Temperature. *IEEE Sens. J*. 2017, 17, 2662–2669. doi:10.1109/JSEN.2017.2684838
130. Sutka, A.; Stingaciu, M.; Mezinskas, G.; Lusic, A. An Alternative Method to Modify the Sensitivity of p-Type  $\text{NiFe}_2\text{O}_4$  Gas Sensor. *J. Mater. Sci*. 2012, 47, 2856–2863. doi:10.1007/s10853-011-6115-2
131. Da Silva, S. W.; Nakagomi, F.; Silva, M. S.; Franco, A.; Garg, V. K.; Oliveira, A. C.; Morais, P. C. Raman Study of Cations' Distribution in  $\text{Zn}_x\text{Mg}_{1-x}\text{Fe}_2\text{O}_4$  Nanoparticles. *J. Nanopart. Res*. 2012, 14, 798. doi:10.1007/s11051-012-0798-4
132. Jiang, Y.; Song, W.; Xie, C.; Wang, A.; Zeng, D.; Hu, M. Electrical Conductivity and Gas Sensitivity to VOCs of V-Doped  $\text{ZnFe}_2\text{O}_4$  Nanoparticles. *Mater. Lett*. 2006, 60, 1374–1378. doi:10.1016/j.matlet.2005.11.032

133. Sutka, A.; Pärna, R.; Mezinskis, G.; Kisand, V. Effects of Co Ion Addition and Annealing Conditions on Nickel Ferrite Gas Response. *Sens. Actuators B*. 2014, 192, 173–180. doi:10.1016/j.snb.2013.10.077
134. Sharma, R.; Thakur, P.; Sharma, P.; Sharma, V. Ferrimagnetic Ni<sup>2+</sup> Doped Mg-Zn Spinel Ferrite Nanoparticles for High Density Information Storage. *J. Alloys Compd.* 2017, 704, 7–17. doi:10.1016/j.jallcom.2017.02.021
135. Arshaka, K.; Twomey, K.; Egan, D. A Ceramic Thick Film Humidity Sensor Based on MnZn Ferrite. *Sensors*. 2002, 2, 50–61. doi:10.3390/s20200050
136. Chen, Z.; Lu, C. Humidity Sensors: A Review of Materials and Mechanisms. *Sen. Lett.* 2005, 3, 274–295. doi:10.1166/sl.2005.045
137. Spasic, I.; Ananiadou, S.; McNaught, J.; Kumar, A. Text Mining and Ontologies in Biomedicine: Making Sense of Raw Text. *Brief. Bioinform.* 2005, 6, 239–251. doi:10.1093/bib/6.3.239
138. Shah, J.; Kotnala, R. K. Humidity Sensing Exclusively by Physisorption of Water Vapor on Magnesium Ferrite. *Sens. Actuators B*. 2012, 171–172, 832–837. doi:10.1016/j.snb.2012.05.079
139. Shah, S. I. H.; Khan, A. Z.; Bokhara, R. H.; Raza, M. A. Exploring the Impediments of Successful ERP Implementation: A Case Study in a Public Organization. *Int. J. Bus. Soc. Sci.* 2011, 2, 289–296.
140. Iftimie, N.; Rezlescu, E.; Popa, P. D.; Rezlescu, N. On the Possibility of the Use of a Nickel Ferrite as Semiconducting Gas Sensor. *J. Optoelectron. Adv. Mater.* 2005, 7, 911–914.
141. Liu, Y. L.; Wang, H.; Yang, Y.; Liu, Z. M.; Yang, H. F.; Shen, G. L.; Yu, R. Q. Hydrogen Sulfide Sensing Properties of NiFe<sub>2</sub>O<sub>4</sub> Nanopowder Doped with Noble Metals. *Sens. Actuators B*. 2004, 102, 148–154. doi:10.1016/j.snb.2004.04.014
142. Srivastava, R.; Yadav, B. C.; Singh, M.; Yadav, T. P. Synthesis, Characterization of Nickel Ferrite and Its Uses as Humidity and LPG Sensors. *J. Inorg. Organomet. Polym.* 2016, 26, 1404–1412. doi:10.1007/s10904-016-0425-4
143. Rezlescu, E.; Iftimie, N.; Popa, P. D.; Rezlescu, N. Porous Nickel Ferrite for Semiconducting Gas Sensor. *J. Phys. Conf. Ser.* 2005, 15, 51. doi:10.1088/1742-6596/15/1/009
144. Yang, L.; Xie, Y.; Zhao, H.; Wu, X.; Wang, Y. Preparation and Gas Sensing Properties of NiFe<sub>2</sub>O<sub>4</sub> semiconductor Materials. *Solid State Electron.* 2005, 49, 1029–1033. doi:10.1016/j.sse.2005.03.022
145. Kazin, A. P.; Rumyantseva, M. N.; Prusakov, V. E.; Suzdalev, I. P.; Maksimov, Y. V.; Imshennik, V. K.; Novochikhin, S. V.; Gaskov, A. M. Microstructure and Gas-Sensing Properties of Nanocrystalline NiFe<sub>2</sub>O<sub>4</sub> Prepared by Spray Pyrolysis. *Inorg. Mater.* 2010, 46, 1254–1259. doi:10.1134/S0020168510110178
146. Iftimie, N.; Rezlescu, E.; Popa, P. D.; Rezlescu, N. Gas Sensitivity of Nanocrystalline Nickel Ferrite. *J. Optoelectron. Adv. Mater.* 2006, 8, 1016.
147. Wang, X. F.; Ma, W.; Jiang, F.; Cao, E. S.; Sun, K. M.; Cheng, L.; Song, X. Z. Prussian Blue Analogue Derived Porous NiFe<sub>2</sub>O<sub>4</sub> Nanocubes for Low-Concentration Acetone Sensing at Low Working Temperature. *Chem. Eng. J.* 2018, 338, 504–512. doi:10.1016/j.cej.2018.01.072
148. Lee, P. Y.; Ishizaka, K.; Suematsu, H.; Jiang, W.; Yatsui, K. Magnetic and Gas Sensing Property of Nanosized NiFe<sub>2</sub>O<sub>4</sub> Powders Synthesized by Pulsed Wire Discharge. *J. Nanopart. Res.* 2006, 8, 29–35. doi:10.1007/s11051-005-5427-z
149. Xiangfeng, C.; Dongli, J.; Yu, G.; Chenmou, Z. Ethanol Gas Sensor Based on CoFe<sub>2</sub>O<sub>4</sub> Nano-Crystallines Prepared by Hydrothermal Method. *Sens. Actuators B*. 2006, 120, 177–181. doi:10.1016/j.snb.2006.02.008
150. Ghosh, P.; Mukherjee, A.; Fu, M.; Chattopadhyay, S.; Mitra, P. Influence of Particle Size on H<sub>2</sub> and H<sub>2</sub>S Sensing Characteristics of Nanocrystalline Nickel Ferrite. *Physica E*. 2015, 74, 570–575. doi:10.1016/j.physe.2015.08.023
151. Rao, P.; Godbole, R. V.; Bhagwat, S. Copper Doped Nickel Ferrite Nano-Crystalline Thin Films: A Potential Gas Sensor towards Reducing Gases. *Mater. Chem. Phys.* 2016, 171, 260–266. doi:10.1016/j.matchemphys.2016.01.016
152. Manikandan, V.; Denardin, J. C.; Vigniselvan, S.; Mane, R. S. Structural, Dielectric and Enhanced Soft Magnetic Properties of Lithium (Li) Substituted Nickel Ferrite (NiFe<sub>2</sub>O<sub>4</sub>) Nanoparticles. *J. Magn. Magn. Mater.* 2018, 465, 634–639. doi:10.1016/j.jmmm.2018.06.059
153. Manikandan, V.; Kim, J. H.; Mirzaei, A.; Kim, S. S.; Vigniselvan, S.; Singh, M.; Chandrasekaran, J. Effect of Temperature on Gas Sensing Properties of Lithium (Li) Substituted (NiFe<sub>2</sub>O<sub>4</sub>) Nickel Ferrite Thin Film. *J. Mol. Struct.* 2019, 1177, 485–490. doi:10.1016/j.molstruc.2018.09.085
154. Manikandan, V.; Tudorache, F.; Petrila, I.; Mane, R. S.; Kuncser, V.; Vasile, B.; Morgan, D.; Vigniselvan, S.; Mirzaei, A. Fabrication and Characterization of Ru-Doped LiCuFe<sub>2</sub>O<sub>4</sub> Nanoparticles and Their Capacitive and Resistive Humidity Sensor Applications. *J. Magn. Magn. Mater.* 2019, 474, 563–569. doi:10.1016/j.jmmm.2018.11.072
155. Manikandan, V.; Singh, M.; Yadav, B. C.; Denardin, J. C. Fabrication of Lithium Substituted Copper Ferrite (Li-CuFe<sub>2</sub>O<sub>4</sub>) Thin Film as an Efficient Gas Sensor at Room Temperature. *J. Sci. Adv. Mater. Devices.* 2018, 3, 145–150. doi:10.1016/j.jsamd.2018.03.008
156. Pandav, R. S.; Tapase, A. S.; Hankare, P. P.; Shelke, G. B.; Patil, D. R. Nanocrystalline Manganese Substituted Nickel Ferrite Thick Films as Ppm Level H<sub>2</sub>S Gas Sensors. *Int. J. Recent Innov. Trends Comput. Commun.* 2015, 3, 5152–5156.
157. Sundari, P. B.; Kumar, E. R.; Ramya, S.; Kamzin, A. S. Structural, Dielectric and Gas Sensing Properties of Mn-Ni Ferrite Nanoparticles. In *Recent Trends in Materials Science and Applications*; Springer: Cham, 2017; pp 135–143.

158. Rao, P.; Godbole, R. V.; Bhagwat, S. Chlorine Gas Sensing Performance of Palladium Doped Nickel Ferrite Thin Films. *J. Magn. Magn. Mater.* 2016, *405*, 219–224. doi:10.1016/j.jmmm.2015.12.065
159. Jiao, W. L.; Zhang, L. Preparation and Gas Sensing Properties for Acetone of Amorphous Ag Modified NiFe<sub>2</sub>O<sub>4</sub> Sensor. *Trans. Nonferrous Met. Soc. China.* 2012, *22*, 1127–1132. doi:10.1016/S1003-6326(11)61294-6
160. Sertkol, M.; Köseoğlu, Y.; Baykal, A.; Kavas, H.; Bozkurt, A.; Toprak, M. S. Microwave Synthesis and Characterization of Zn-Doped Nickel Ferrite Nanoparticles. *J. Alloys Compd.* 2009, *486*, 325–329. doi:10.1016/j.jallcom.2009.06.128
161. Sutka, A.; Mezinskis, G.; Lusiš, A.; Stingaciū, M. Gas Sensing Properties of Zn-Doped p-Type Nickel Ferrite. *Sens. Actuators B.* 2012, *171–172*, 354–360. doi:10.1016/j.snb.2012.04.059
162. Sutka, A.; Mezinskis, G.; Lusiš, A.; Jakovlevs, D. Influence of Iron Non-Stoichiometry on Spinel Zinc Ferrite Gas Sensing Properties. *Sens. Actuators B.* 2012, *171–172*, 204–209. doi:10.1016/j.snb.2012.03.012
163. Bagade, A. A.; Ganbavle, V. V.; Mohite, S. V.; Dongale, T. D.; Sinha, B. B.; Rajpure, K. Y. Assessment of Structural, Morphological, Magnetic and Gas Sensing Properties of CoFe<sub>2</sub>O<sub>4</sub> Thin Films. *J. Colloid Interface Sci.* 2017, *497*, 181–192. doi:10.1016/j.jcis.2017.02.067
164. Patil, R. P.; Nikam, P. N.; Patil, S. B.; Talap, P. D.; Patil, D. R.; Hankare, P. P. Structural, Magnetic and Gas Sensing Application of Novel Polyol Route Synthesized Cobalt Ferrite. *Sen. Lett.* 2015, *13*, 785–790. doi:10.1166/sl.2015.3522
165. Singh, S.; Singh, A.; Yadav, B. C.; Tandon, P. Synthesis, Characterization, Magnetic Measurements and Liquefied Petroleum Gas Sensing Properties of Nanostructured Cobalt Ferrite and Ferric Oxide. *Mater. Sci. Semicond. Process.* 2014, *23*, 122–135. doi:10.1016/j.mssp.2014.02.048
166. Bagade, A. A.; Rajpure, K. Y. Development of CoFe<sub>2</sub>O<sub>4</sub> Thin Films for Nitrogen Dioxide Sensing at Moderate Operating Temperature. *J. Alloys Compd.* 2016, *657*, 414–421. doi:10.1016/j.jallcom.2015.10.115
167. Leroux, C.; Madigou, V.; Bendahan, M.; Mliki, N.; Ajroudi, L. P1.8.5 Cobalt Ferrite, a New Gas Sensing Material. *Tagungsband. IMCS 2012 – The 14th International Meeting on Chemical Sensors.* 2012, 1119–1121.
168. Raut, S. D.; Awasarmol, V. V.; Ghule, B. G.; Shaikh, S. F.; Gore, S. K.; Sharma, R. P.; Pawar, P. P.; Mane, R. S. Enhancement in Room-Temperature Ammonia Sensor Activity of Size-Reduced Cobalt Ferrite Nanoparticles on  $\gamma$ -Irradiation. *Mater. Res. Express.* 2018, *5*, 065035. doi:10.1088/2053-1591/aac99d
169. Gedam, N. N.; Padole, P. R.; Rithe, S. K.; Chaudhari, G. N. Ammonia Gas Sensor Based on a Spinel Semiconductor, Co<sub>0.8</sub>Ni<sub>0.2</sub>Fe<sub>2</sub>O<sub>4</sub> Nanomaterial. *J. Sol-Gel Sci. Technol.* 2009, *50*, 296–300. doi:10.1007/s10971-009-1942-1
170. Bagade, A. A.; Rajpure, K. Y. Studies on NO<sub>2</sub> Gas Sensing Properties of Sprayed Co<sub>1-x</sub>MnxFe<sub>2</sub>O<sub>4</sub> (0  $\leq$  x  $\leq$  0.5) Spinel Ferrite Thin Films. *Ceram. Int.* 2015, *41*, 7394–7401. doi:10.1016/j.ceramint.2015.02.051
171. Devi, P. I.; Rajkumar, N.; Renganathan, B.; Sastikumar, D.; Ramachandran, K. Ethanol Gas Sensing of Mn-Doped CoFeO Nanoparticles. *IEEE Sens. J.* 2011, *11*, 1395–1402. doi:10.1109/JSEN.2010.2093881
172. Abdel Maksoud, M. I. A.; El-Sayyad, G. S.; Ashour, A. H.; El-Batal, A. I.; Abd-Elmonem, M. S.; Hendawy, H. A. M.; Abdel-Khalek, E. K.; Labib, S.; Abdeltwab, E.; El-Okri, M. M. Synthesis and Characterization of Metals-Substituted Cobalt Ferrite [M<sub>x</sub>Co<sub>1-x</sub>Fe<sub>2</sub>O<sub>4</sub>; (M = Zn, Cu and Mn; x = 0 and 0.5)] Nanoparticles as Antimicrobial Agents and Sensors for Anagrelide Determination in Biological Samples. *Mater. Sci. Eng. C.* 2018, *92*, 644–656. doi:10.1016/j.msec.2018.07.007
173. Khandekar, M. S.; Tarwal, N. L.; Patil, J. Y.; Shaikh, F. I.; Mulla, I. S.; Suryavanshi, S. S. Liquefied Petroleum Gas Sensing Performance of Cerium Doped Copper Ferrite. *Ceram. Int.* 2013, *39*, 5901–5907. doi:10.1016/j.ceramint.2013.01.010
174. Kumar, E. R.; Kamzin, A. S.; Janani, K. Effect of Annealing on Particle Size, Microstructure and Gas Sensing Properties of Mn Substituted CoFe<sub>2</sub>O<sub>4</sub> Nanoparticles. *J. Magn. Magn. Mater.* 2016, *417*, 122–129. doi:10.1016/j.jmmm.2016.05.072
175. Xu, Y.; Sun, D.; Hao, H.; Gao, D.; Sun, Y. Non-Stoichiometric Co (II), Ni (II), Zn (II)-Ferrite Nanospheres: Size Controllable Synthesis, Excellent Gas-Sensing and Magnetic Properties. *RSC Adv.* 2016, *6*, 98994–99002. doi:10.1039/C6RA21990J
176. Liang, Y. C.; Liu, S. L.; Hsia, H. Y. Physical Synthesis Methodology and Enhanced Gas Sensing and Photoelectrochemical Performance of 1D Serrated Zinc Oxide–Zinc Ferrite Nanocomposites. *Nanoscale Res. Lett.* 2015, *10*, 1–7. doi:10.1186/s11671-015-1059-0
177. Darshane, S. L.; Deshmukh, R. G.; Suryavanshi, S. S.; Mulla, I. S. Gas-Sensing Properties of Zinc Ferrite Nanoparticles Synthesized by the Molten-Salt Route. *J. Am. Ceram. Soc.* 2008, *91*, 2724–2726. doi:10.1111/j.1551-2916.2008.02475.x
178. Cao, Y.; Jia, D.; Hu, P.; Wang, R. One-Step Room-Temperature Solid-Phase Synthesis of ZnFe<sub>2</sub>O<sub>4</sub> Nanomaterials and Its Excellent Gas-Sensing Property. *Ceram. Int.* 2013, *39*, 2989–2994. doi:10.1016/j.ceramint.2012.09.076
179. Tyagi, S.; Batra, N.; Paul, A. K. Influence of Temperature on Reducing Gas Sensing Performance of Nanocrystalline Zinc Ferrite. *Trans. Indian Inst. Met.* 2015, *68*, 707–713. doi:10.1007/s12666-014-0503-7
180. Zhu, H.; Gu, X.; Zuo, D.; Wang, Z.; Wang, N.; Yao, K. Microemulsion-Based Synthesis of Porous Zinc Ferrite Nanorods and Its Application in a Room-Temperature Ethanol Sensor. *Nanotechnology.* 2008, *19*, 405503. doi:10.1088/0957-4484/19/40/405503
181. Mukherjee, K.; Majumder, S. B. Promising Methane-Sensing Characteristics of Hydrothermal Synthesized Magnesium Zinc Ferrite Hollow Spheres. *Scr. Mater.*

- 2012, 67, 617–620. doi:10.1016/j.scriptamat.2012.06.025
182. Bharti, D. C.; Mukherjee, K.; Majumder, S. B. Wet Chemical Synthesis and Gas Sensing Properties of Magnesium Zinc Ferrite Nano-Particles. *Mater. Chem. Phys.* 2010, 120, 509–517. doi:10.1016/j.matchemphys.2009.11.050
183. Karmakar, M.; Das, P.; Pal, M.; Mondal, B.; Majumder, S. B.; Mukherjee, K. Acetone and Ethanol Sensing Characteristics of Magnesium Zinc Ferrite Nano-Particulate Chemi-Resistive Sensor. *J. Mater. Sci.* 2014, 49, 5766–5771. doi:10.1007/s10853-014-8302-4
184. Maity, A.; Mukherjee, K.; Majumder, S. B. Addressing the Cross-Sensitivity of Magnesium Zinc Ferrite towards Reducing Gas Sensing Using Pattern Recognition Techniques. *Sens. Lett.* 2012, 10, 916–920. doi:10.1166/sl.2012.2329
185. Mukherjee, K.; Majumder, S. B. Reducing Gas Sensing Behaviour of Nano-Crystalline Magnesium–Zinc Ferrite Powders. *Talanta*. 2010b, 81, 1826–1832. doi:10.1016/j.talanta.2010.03.042
186. Jain, A.; Baranwal, R. K.; Bharti, A.; Vakil, Z.; Prajapati, C. S. Study of Zn-Cu Ferrite Nanoparticles for LPG Sensing. *Sci. World J.* 2013, 2013, 1–7. doi:10.1155/2013/790359
187. Singh, S.; Yadav, B. C.; Prakash, R.; Bajaj, B.; Lee, J. R. Synthesis of Nanorods and Mixed Shaped Copper Ferrite and Their Applications as Liquefied Petroleum Gas Sensor. *Appl. Surf. Sci.* 2011, 257, 10763–10770. doi:10.1016/j.apsusc.2011.07.094
188. Singh, S.; Yadav, B. C.; Gupta, V. D.; Dwivedi, P. K. Investigation on Effects of Surface Morphologies on Response of LPG Sensor Based on Nanostructured Copper Ferrite System. *Mater. Res. Bull.* 2012, 47, 3538–3547. doi:10.1016/j.materresbull.2012.06.064
189. Chapelle, A.; Oudrhiri-Hassani, F.; Presmanes, L.; Barnabé, A.; Tailhades, P. CO<sub>2</sub> Sensing Properties of Semiconducting Copper Oxide and Spinel Ferrite Nanocomposite Thin Film. *Appl. Surf. Sci.* 2010, 256, 4715–4719. doi:10.1016/j.apsusc.2010.02.079
190. Chapelle, A.; El Younsi, I.; Vitale, S.; Thimont, Y.; Nelis, T.; Presmanes, L.; Barnabé, A.; Tailhades, P. Improved Semiconducting CuO/CuFe<sub>2</sub>O<sub>4</sub> Nanostructured Thin Films for CO<sub>2</sub> Gas Sensing. *Sens. Actuators B.* 2014, 204, 407–413. doi:10.1016/j.snb.2014.07.088
191. Sumangala, T. P.; Thimont, Y.; Baco-Carles, V.; Presmanes, L.; Bonningue, C.; Pasquet, I.; Tailhades, P.; Barnabé, A. Study on the Effect of Cuprite Content on the Electrical and CO<sub>2</sub> Sensing Properties of Cuprite-Copper Ferrite Nanopowder Composites. *J. Alloys Compd.* 2017, 695, 937–943. doi:10.1016/j.jallcom.2016.10.197
192. Chapelle, A.; Yaacob, M. H.; Pasquet, I.; Presmanes, L.; Barnabé, A.; Tailhades, P.; Plessis, J. D.; Kalantar-Zadeh, K. Structural and Gas-Sensing Properties of CuO–Cu<sub>x</sub>Fe<sub>3–x</sub>O<sub>4</sub> Nanostructured Thin Films. *Sens. Actuators B.* 2011, 153, 117–124. doi:10.1016/j.snb.2010.10.018
193. Haija, M. A.; Abu-Hani, A. F.; Hamdan, N.; Stephen, S.; Ayesh, A. I. Characterization of H<sub>2</sub>S Gas Sensor Based on CuFe<sub>2</sub>O<sub>4</sub> Nanoparticles. *J. Alloys Compd.* 2017, 690, 461–468. doi:10.1016/j.jallcom.2016.08.174
194. Singh, A.; Singh, A.; Singh, S.; Tandon, P. Fabrication of Copper Ferrite Porous Hierarchical Nanostructures for an Efficient Liquefied Petroleum Gas Sensor. *Sens. Actuators B.* 2017, 244, 806–814. doi:10.1016/j.snb.2017.01.069
195. Khandekar, M. S.; Tarwal, N. L.; Mulla, I. S.; Suryavanshi, S. S. Nanocrystalline Ce Doped CoFe<sub>2</sub>O<sub>4</sub> as an Acetone Gas Sensor. *Ceram. Int.* 2014, 40, 447–452. doi:10.1016/j.ceramint.2013.06.021
196. Kumar, E. R.; Jayaprakash, R.; Devi, G. S.; Reddy, P. S. P. Magnetic, Dielectric and Sensing Properties of Manganese Substituted Copper Ferrite Nanoparticles. *J. Magn. Magn. Mater.* 2014, 355, 87–92. doi:10.1016/j.jmmm.2013.11.051
197. Manikandan, V.; Li, X.; Mane, R. S.; Chandrasekaran, J. Room Temperature Gas Sensing Properties of Sn-Substituted Nickel Ferrite (NiFe<sub>2</sub>O<sub>4</sub>) Thin Film Sensors Prepared by Chemical Co-precipitation Method. *J. Electron. Mater.* 2018, 47, 3403–3408. doi:10.1007/s11664-018-6295-5
198. Zhao, C.; Lan, W.; Gong, H.; Bai, J.; Ramachandran, R.; Liu, S.; Wang, F. Highly Sensitive Acetone-Sensing Properties of Pt-Decorated CuFe<sub>2</sub>O<sub>4</sub> Nanotubes Prepared by Electrospinning. *Ceram. Int.* 2018, 44, 2856–2863. doi:10.1016/j.ceramint.2017.11.032
199. Tianshu, Z.; Hing, P.; Jiancheng, Z.; Lingbing, K. Ethanol-Sensing Characteristics of Cadmium Ferrite Prepared by Chemical Coprecipitation. *Mater. Chem. Phys.* 1999, 61, 192–198. doi:10.1016/S0254-0584(99)00133-9
200. Gadkari, A. B.; Shinde, T. J.; Vasambekar, P. N. Ethanol Sensor Based on Nanocrystallite Cadmium Ferrite. *AIP Conf. Proc.* 2015, 1665, 050001.
201. Kotresh, S.; Ravikiran, Y. T.; Tiwari, S. K.; Kumari, S. V. Polyaniline–Cadmium Ferrite Nanostructured Composite for Room-Temperature Liquefied Petroleum Gas Sensing. *J. Electron. Mater.* 2017, 46, 5240–5247. doi:10.1007/s11664-017-5535-4
202. Chethan, B.; Ravikiran, Y. T.; Vijayakumari, S. C.; Rajprakash, H. G.; Thomas, S. Nickel Substituted Cadmium Ferrite as Room Temperature Operable Humidity Sensor. *Sens. Actuators A.* 2018, 280, 466–474. doi:10.1016/j.sna.2018.08.017
203. Liu, X.; Xu, Z.; Shen, Y. A New Type Ethanol Sensing Material on CdFe<sub>2</sub>O<sub>4</sub> Semiconductor. *J. Yunnan Univ. Nat. Sci.* 1997, 19, 147–149.
204. Godbole, R.; Rao, P.; Bhagwat, S. Magnesium Ferrite Nanoparticles: A Rapid Gas Sensor for Alcohol. *Mater. Res. Express.* 2017, 4, 025032. doi:10.1088/2053-1591/aa5ec7
205. Patil, J. Y.; Nadargi, D. Y.; Mulla, I. S.; Suryavanshi, S. S. Cerium Doped MgFe<sub>2</sub>O<sub>4</sub> Nanocomposites: highly Sensitive and Fast Response-Recoverable Acetone Gas Sensor. *Heliyon.* 2019, 5, e01489. doi:10.1016/j.heliyon.2019.e01489
206. Darshane, S.; Mulla, I. S. Influence of Palladium on Gas-Sensing Performance of Magnesium Ferrite Nanoparticles. *Mater. Chem. Phys.* 2010, 119, 319–323. doi:10.1016/j.matchemphys.2009.09.004

207. Kotnala, R. K.; Shah, J.; Singh, B.; Kishan, H.; Singh, S.; Dhawan, S. K.; Sengupta, A. Humidity Response of Li-Substituted Magnesium Ferrite. *Sens. Actuators B*. 2008, *129*, 909–914. doi:10.1016/j.snb.2007.10.002
208. Rathore, D.; Mitra, S. MnFe<sub>2</sub>O<sub>4</sub> as a Gas Sensor towards SO<sub>2</sub> and NO<sub>2</sub> Gases. *AIP Conf. Proc.* 2016, *1728*, 020166.
209. Vignesh, R. H.; Sankar, K. V.; Amaresh, S.; Lee, Y. S.; Selvan, R. K. Synthesis and Characterization of MnFe<sub>2</sub>O<sub>4</sub> Nanoparticles for Impedometric Ammonia Gas Sensor. *Sens. Actuators B*. 2015, *220*, 50–58. doi:10.1016/j.snb.2015.04.115
210. Köseoğlu, Y. A Simple Microwave-Assisted Combustion Synthesis and Structural, Optical and Magnetic Characterization of ZnO Nanoplatelets. *Ceram. Int.* 2014, *40*, 4673–4679. doi:10.1016/j.ceramint.2013.09.008
211. Mangalaraja, R. V.; Ananthakmar, S.; Manohar, P.; Gnanam, F. D.; Awano, M. Characterization of Mn<sub>0.8</sub>Zn<sub>0.2</sub>Fe<sub>2</sub>O<sub>4</sub> Synthesized by Flash Combustion Technique. *Mater. Sci. Eng. A*. 2004, *367*, 301–305. doi:10.1016/j.msea.2003.10.283
212. Costa, A. C. F.; Morelli, M. R.; Kiminami, R. H. Combustion Synthesis: Effect of Urea on the Reaction and Characteristics of Ni-Zn Ferrite Powders. *J. Mater. Synth. Process.* 2001, *9*, 347–352. doi:10.1023/A:1016356623401
213. Xue, H.; Li, Z.; Wang, X.; Fu, X. Facile Synthesis of Nanocrystalline Zinc Ferrite via a Self-Propagating Combustion Method. *Mater. Lett.* 2007, *61*, 347–350. doi:10.1016/j.matlet.2006.04.061
214. Yu, L.; Cao, S.; Liu, Y.; Wang, J.; Jing, C.; Zhang, J. Thermal and Structural Analysis on the Nanocrystalline NiCuZn Ferrite Synthesis in Different Atmospheres. *J. Magn. Magn. Mater.* 2006, *301*, 100–106. doi:10.1016/j.jmmm.2005.06.020
215. Junliang, L.; Wei, Z.; Cuijing, G.; Yanwei, Z. Synthesis and Magnetic Properties of Quasi-Single Domain M-Type Barium Hexaferrite Powders via Sol-Gel Auto-Combustion: Effects of pH and the Ratio of Citric Acid to Metal Ions (CA/M). *J. Alloys Compd.* 2009, *479*, 863–869. doi:10.1016/j.jallcom.2009.01.081
216. Thakur, P.; Sharma, R.; Kumar, M.; Katyal, S. C.; Negi, N. S.; Thakur, N.; Sharma, V.; Sharma, P. Superparamagnetic La Doped Mn-Zn Nano Ferrites: Dependence on Dopant Content and Crystallite Size. *Mater. Res. Express.* 2016, *3*, 075001. doi:10.1088/2053-1591/3/7/075001
217. Valenzuela, R.; Fuentes, M. C.; Parra, C.; Baeza, J.; Duran, N.; Sharma, S. K.; Knobel, M.; Freer, J. Influence of Stirring Velocity on the Synthesis of Magnetite Nanoparticles (Fe<sub>3</sub>O<sub>4</sub>) by the co-Precipitation Method. *J. Alloys Compd.* 2009, *488*, 227–231. doi:10.1016/j.jallcom.2009.08.087
218. Salazar-Alvarez, G.; Olsson, R. T.; Sort, J.; Macedo, W. A. A.; Ardisson, J. D.; Baró, M. D.; Gedde, U. W.; Nogués, J. Enhanced Coercivity in Co-Rich Near-Stoichiometric Co<sub>x</sub>Fe<sub>3-x</sub>O<sub>4+δ</sub> Nanoparticles Prepared in Large Batches. *Chem. Mater.* 2007, *19*, 4957–4963. doi:10.1021/cm070827t
219. Abdel-Latif, I. A. Fabrication of Nano-Size Nickel Ferrites for Gas Sensors Applications. *J. Phys.* 2012, *1*, 50–53.